UNIVERSITY OF THESSALY

SCHOOL OF ENGINEERING

DEPARTMENT OF MECHANICAL ENGINEERING

«Electrochemical detection of ascorbic and uric acid using platinum and palladium based catalysts»

By

Apostolos Kravvaris & Dimitrios Tsakiridis

Supervisor

Prof. Tsiakaras Panagiotis

Submitted in fulfillment of the requirements for the Diploma in the Department of

Mechanical Engineering of the University of Thessaly

VOLOS, 2018

ΠΑΝΕΠΙΣΤΗΜΙΟ ΘΕΣΣΑΛΙΑΣ

ΠΟΛΥΤΕΧΝΙΚΗ ΣΧΟΛΗ

ΤΜΗΜΑ ΜΗΧΑΝΟΛΟΓΩΝ ΜΗΧΑΝΙΚΩΝ

«**Ηλεκτροχημική ανίχνευση ασκορβικού και ουρικού οξέος με τη χρήση καταλυτών με βάση πλατίνα και παλλάδιο**»

Υπό

Απόστολου Κράββαρη & Δημητρίου Τσακιρίδη

Επιβλέπων

Καθηγητής Τσιακάρας Παναγιώτης

Υπεβλήθη για την εκπλήρωση μέρους των απαιτήσεων για την απόκτηση του

Διπλώματος Μηχανολόγου Μηχανικού

ΒΟΛΟΣ, 2018

Η έγκριση της διπλωματικής εργασίας από το Τμήμα Μηχανολόγων Μηχανικών Βιομηχανίας της Πολυτεχνικής Σχολής του Πανεπιστημίου Θεσσαλίας δεν υποδηλώνει αποδοχή των απόψεων του συγγραφέα (Ν. 5343/32 αρ. 202 παρ. 2).

Εγκρίθηκε από τα Μέλη της Τριμελούς Εξεταστικής Επιτροπής:

1st Examiner: Dr Tsiakaras Panagiotis (Supervisor)

Professor of Department of Mechanical Engineering,

School of Engineering

University of Thessaly

2nd Examiner: Dr Michael Agoras

Assistant Professor of Department of Mechanical Engineering,

School of Engineering

University of Thessaly

3rd Examiner: Dr Angeliki Brouzgou

Senior researcher and Teaching Staff of Department of Mechanical Engineering,

School of Engineering

University of Thessaly

ABSTRACT

Ascorbic acid, or vitamin C as it is more commonly known and uric acid are compounds of great significance for various physiological and biochemical processes. In the human organism sufficient amounts of ascorbic acid are required for strong immunity, while deficiency of this vitamin can lead to numerous diseases. High uric acid levels on the other hand are linked to many clinical conditions. Regulating the concentration of ascorbic and uric acid in the body is an effective way of diagnosis, prevention and treatment of a diversity of diseases.

As an immediate result, reliable, rapid, smart, flexible and low cost devices need to be developed for ascorbic and uric acid detection. For this objective, the interest of the scientific community concentrates on developing electrochemical sensors, which convert electrochemical information into exploitable analytically signal. These types of sensors represent a rapidly growing subject and could find a wide range of applications in clinical, industrial and environmental fields. Various studies of metal-catalysts, such as Pt, Pd, Au, Ru and Bi demonstrate promising potential in electroanalysis and indicate that these materials can be used for sensor designing. Especially, Pt and Pd type catalyst has shown remarkable catalytic activity towards ascorbic and uric acid oxidation.

In this current thesis, the catalytic effect of Pt(20%wt)/graphitized carbon and Pd(20wt%)/Vulcan-XC72 for the oxidation of 0.5mM ascorbic and 0.5mM uric acid in physiological-buffer solution of 7.3 pH is discussed. Electrochemical techniques, such as cyclic voltammetry and chronoamperometry are employed. It is found that Pt(20%wt)/graphitized carbon exhibit great electrochemical activity towards ascorbic and uric acid oxidation, whereas the catalytic activity of Pd(20wt%)/Vulcan-XC72 was significantly lower in both cases. The durability of the Pt(20%wt)/graphitized carbon catalyst was notable higher for the ascorbic acid solution, rather than the uric acid mixture, while Pd(20wt%)/Vulcan-XC72 illustrated relatively low durability. The stability of both catalysts was satisfying and the increase in temperature causes a visible increase in the anodic peak current of all cyclic voltammograms.

ΠΕΡΙΛΗΨΗ

Το ασκορβικό οξύ, ή βιταμίνη C όπως είναι ευρέως γνωστή και το ουρικό οξύ είναι στοιχεία μεγάλης σημασίας για πλήθος φυσικών και βιοχημικών διαδικασιών. Στον ανθρώπινο οργανισμό, επαρκή ποσότητα ασκορβικού οξέος είναι απαραίτητη για δυνατή ανοσία, ενώ η έλλειψη της βιταμίνης αυτής μπορεί να οδηγήσει σε πολυάριθμες ασθένειες. Υψηλά ποσοστά ουρικού οξέος από την άλλη συνδέονται με πολλές κλινικές καταστάσεις. Η εξισορρόπηση της συγκέντρωσης ασκορβικού και ουρικού οξέος στο σώμα είναι ένας αποτελεσματικός τρόπος διάγνωσης, πρόληψης και θεραπείας πολλών ασθενειών.

Ως άμεσο αποτέλεσμα, αξιόπιστοι, γρήγοροι, έξυπνοι, εφαρμόσιμοι και χαμηλού κόστους αισθητήρες χρειάζεται να αναπτυχθούν για την ανίχνευση ασκορβικού και ουρικού οξέος. Για τον σκοπό αυτό, το ενδιαφέρον της επιστημονικής κοινότητας συγκεντρώνεται στην ανάπτυξη ηλεκτροχημικών αισθητήρων, οι οποίοι μετατρέπουν την ηλεκτροχημική πληροφορία σε εκμεταλλεύσιμο αναλυτικό σήμα. Αυτού του τύπου οι ανιχνευτές αντιπροσωπεύουν ένα ταχέως αναπτυσσόμενο θέμα, έχοντας ευρύ φάσμα εφαρμογών σε κλινικούς, βιομηχανικούς και περιβαλλοντικούς τομείς. Εκτεταμένες έρευνες σε μεταλλικούς καταλυτές, όπως Pt, Pd, Au, Ru και Bi επιδεικνύουν πολλά υποσχόμενες δυνατότητες στη ηλεκτροανάλυση και έδειξαν ότι αυτά τα υλικά μπορούν να χρησιμοποιηθούν για τον σχεδιασμό αισθητήρα. Ειδικότερα, καταλύτες με βάση το Pt και το Pd έχουν παρουσιάσει αξιοσημείωτη καταλυτική δράση προς τη οξείδωση του ασκορβικού και ουρικού οξέος.

Στην παρούσα διπλωματική παρουσιάζεται η επίδραση των καταλυτών Pt(20%wt)/graphitized carbon και Pd(20wt%)/Vulcan-XC72 για την οξείδωση 0.5 mM ασκορβικού οξέος και 0.5mM ουρικού οξέος σε φυσιολογικό ορό με 7.3 pH. Βρέθηκε ότι ο καταλύτης Pt(20%wt)/graphitized carbon επιδεικνύει καλή ηλεκτροχημική δράση προς τη οξείδωση του ασκορβικού και ουρικού οξέος, ενώ η καταλυτική δράση του Pd(20wt%)/Vulcan-XC72 ήταν σημαντικά χαμηλότερη και στις δύο περιπτώσεις. Η ανθεκτικότητα του Pt(20%wt)/graphitized carbon ήταν αξιοσημείωτα υψηλή προς το διάλυμα του ασκορβικού οξέος, σε σχέση με αυτό του ουρικού οξέος, ενώ το Pd(20wt%)/Vulcan-XC72 παρουσίασε σχετικά χαμηλή ανθεκτικότητα. Η σταθερότητα και των δύο καταλυτών ήταν ικανοποιητική και η άνοδος της θερμοκρασίας προκάλεσε αξιοσημείωτη αύξηση στην ανώτατη τιμή ρεύματος ανόδου οξείδωσης σε όλα τα κυκλικά βολταμογραφήματα.

ACKNOWLEDGEMENTS

First and foremost, we would like to express our most sincere gratitude to Professor Dr Panagiotis Tsiakaras for giving us the opportunity to involve in this project at the laboratory of alternative energy conversion systems of our department, where the experiments took place. His constant interest, commitment, guidance and support, meant a great deal to us and the way he influenced our way of thinking and helped us grow as an individual, are values that we will carry with us for the rest of our lives.

The accomplishment of this thesis is owed to Dr Angeliki Brouzgou and Dr Sotiria Kontou. Their knowledge, patience and assistance were essential for the consummation of this work. We also could not neglect to thank our colleague Marina Sdougkou for the countless hours spent together conducting experiments at the laboratory. Furthermore, we feel obligated to thank the members of the examination committee, for their time and useful advice.

Last but certainly not least, we would like to thank our family and our parents, without whom we would never have make it this far. Their patience and understanding helped us to cope with many problems we encountered, not only during the composition of this thesis, but throughout our study at the Department of Mechanical Engineering in University of Thessaly. Their love and moral support exceed by far any financial endorsement. We dedicate our work to them.

Apostolos Kravvaris

Dimitrios Tsakiridis

ΕΥΧΑΡΙΣΤΙΕΣ

Πρώτα απ' όλα, θα θέλαμε να εκφράσουμε την πιο ειλικρινή ευγνωμοσύνη μας στο καθηγητή κύριο Παναγιώτη Τσιακάρα που μας έδωσε την ευκαιρία να εμπλακούμε στη μελέτη αυτή στο εργαστήριο εναλλακτικών συστημάτων παραγωγής ενέργειας του τμήματός μας, στο οποίο έγιναν τα πειράματα. Το διαρκές του ενδιαφέρον, η αφοσίωση, η καθοδήγηση και η υποστήριξη του σημαίνουν πολλά για μας και ο τρόπος που επηρέασε τον τρόπο σκέψης μας και μας βοήθησε με αυτόν τον τρόπο να εξελιχθούμε σαν άτομα, είναι αξίες που θα κουβαλάμε μαζί μας για το υπόλοιπο της ζωής μας.

Η ολοκλήρωση της διπλωματικής αυτής είναι οφειλόμενη στην Δρ. Αγγελική Μπρούζγου και Δρ. Σωτηρία Κόντου. Η γνώση, η υπομονή και η βοήθεια τους ήταν πολύ σημαντική για την πέρας της εργασίας αυτής. Επίσης δεν θα μπορούσαμε να παραβλέψουμε να ευχαριστήσουμε τη συνάδελφο Μαρίνα Σδούγκου για τις αμέτρητες ώρες που περάσαμε μαζί κάνοντας τα πειράματα στο εργαστήριο. Ακόμα, θα θέλαμε να ευχαριστήσουμε τα μέλη της εξεταστικής επιτροπής, για τον χρόνο τους και τις χρήσιμες συμβουλές τους.

Τέλος, θα θέλαμε να ευχαριστήσουμε την οικογένεια και τους γονείς μας, χωρίς τους οποίους δεν θα τα καταφέρναμε να φτάσουμε μέχρι εδώ. Η υπομονή και η κατανόηση τους μας βοήθησαν να ανταπεξέλθουμε σε πολλά προβλήματα που αντιμετωπίσαμε , όχι μόνο στην ολοκλήρωση της διπλωματικής αυτής αλλά σε όλη της πορεία των σπουδών μας στο Πανεπιστήμιο Θεσσαλίας. Η αγάπη τους και η ηθική τους ενθάρρυνση ήταν πιο σημαντική από κάθε οικονομική υποστήριξη. Τους την αφιερώνουμε.

Απόστολος Κράββαρης

Δημήτριος Τσακιρίδης

CONTENTS

CHAPTER 1: Theoretical Background 1

1.1 Introduction 1

1.2 Electrochemical detection of ascorbic acid and its importance 2

1.3 Electrochemical detection of uric acid and its importance 9

CHAPTER 2: Electrochemical devices 15

2.1 Fuel Cell 15

2.2 Batteries 17

2.3 Supercapacitors 22

2.4 Electrolyzers 25

2.5 Electrochemical sensors 27

2.5.1 Fundamental properties 28

2.5.2 Potentiometric Sensors 32

2.5.3 Conductometric Sensors 33

CHAPTER 3: Electrochemical amperometric sensors 35

3.1 Basic theory 35

3.1.1 Chemically modified electrodes 37

3.1.2 Microelectrodes 38

3.1.3 Screen printed electrodes. 38

3.2 Electrochemical thermodynamics and kinetics 39

3.2.1 Faraday's Law 39

3.2.2 Limiting Current 40

3.2.3 Nernst Equation 41

3.2.4 Butler-Volmer Equation *43*

3.2.5 Tafel Equation *44*

3.2.6 Koutecky-Levich Equation *47*

CHAPTER 4: Experimental Part **49**

4.1 Experimental techniques 49

4.1.1 Transmission electron microscopy *49*

4.1.2 Cyclic Voltammetry *50*

4.1.3 Chronoamperometry *51*

4.1.4 Rotating disk electrode *52*

4.2 Experimental Procedure 54

CHAPTER 5: Results and discussion **57**

5.1 Pt(20%wt)/graphitized carbon electrocatalyst 57

5.1.1 Physicochemical characterization *57*

5.1.2 Electrochemical characterization *58*

5.2 Pd (20%wt)/Vulcan-XC72 electrocatalyst 68

5.2.1 Physicochemical characterization *68*

5.2.2 Electrochemical characterization *68*

CHAPTER 6: Conclusions and future perspectives **77**

References **79**

CHAPTER 1: Theoretical Background

1.1 Introduction

Advances in electrochemistry have provided efficient and analytical systems characterized by instrumental simplicity, moderate cost, portability and short analysis time. Electrochemical techniques introduce promising methods for specific application, as they have shown to be exceptional for the detection of pharmaceutical compounds in difference matrices, as many of the active constituents can be easily oxidized or reduced. It can be fairly assumed that the mechanisms involving oxidation and reduction taking place at the electrode and in the body share the same principles, due to the similarity of biological and electrochemical reactions.

Deposition of catalytic pastes on electrode surface has great significance as analytical tool for electrochemical detection. Utilizing an electro-catalyst improve the activity, sensitivity, stability and selectivity, values essential for the determination of electroactive molecules. This thesis presents the effect of catalytic paste deposition of Pd(20wt%)/VulcanXC-72 and Pt(20%wt)/graphitized carbon.

This thesis is consisted of 6 chapters. The first chapter includes the introduction, in which the importance of ascorbic and uric acid to human organism is pointed out. A literature review of ascorbic and uric acid catalysts for sensors is also included. Second chapter presents the main applications of the electrochemical cell technology, such as fuel cells, batteries, supercapacitors, electrolyzers, concluding to the electrochemical sensors. In succession, third chapter focuses on electrochemical amperometric sensors and the basic principles of electrochemistry applied to describe their function. Fourth chapter refers to the experimental techniques and procedure followed to determinate the electrochemical behavior of the examined catalysts and chapter five is a demonstration of the results obtained. Finally, chapter six includes the conclusions and future suggestions.

1.2 Electrochemical detection of ascorbic acid and its importance

Ascorbic acid ($C_6H_8O_6$), also known as vitamin C, is a hexanoic sugar acid with two dissociable protons (Fig. 1.1). Body requires vitamin C for numerous physiological functions, such as lowering blood cholesterol levels, contributing to the synthesis of amino acids and catecholamines, which regulate the nervous system and assisting in the metabolism of important components like tyrosine, folic acid and tryptophan. Its presence is mandatory for the formation and maintenance of collagen, which promotes tissue growth, wound healing, bone strength and aids in the formation of neurotransmitters and increases the absorption of iron in the gut. As an antioxidant, it protects the body from free radicals induced diseases, pollutants and it can break down histamine, which is the inflammatory component that can triggers many allergic reactions [1, 2].

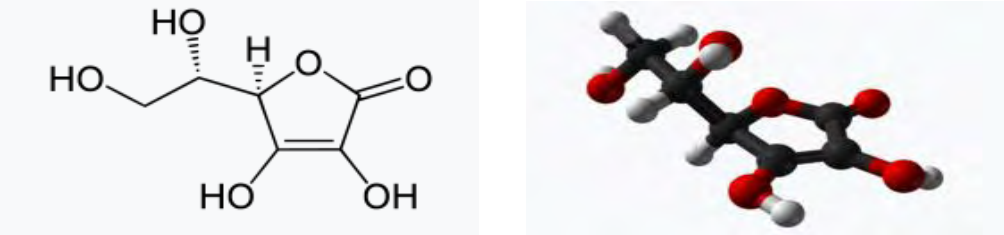

Figure 1.1. Chemical and Molecular structure of ascorbic acid [3].

Vitamin C therapy is effective in the treatment of many different infections, ranging from the common cold and flu, to hepatitis and HIV. Doses of vitamin C are also used for the treatment and prevention of various disorders, such as diabetes, glaucoma, cataracts, stroke, heart diseases, macular degeneration, atherosclerosis and experimentally to cancer, while deficiency of this vitamin can lead to scurvy, infections, anemia, bleeding gums, muscle degeneration, poor wound healing, atherosclerotic plaques, capillary hemorrhaging and neurotic disturbances. Infections can decrease vitamin C stored in the body, making the immune system weaker to possible threats, as it is required for strong immunity.

Micronutrients such as vitamins appear to have preventive properties against cancer [4]. Ascorbate has been tested as therapy for cancer at experimental stage. Recent studies

provide rationale for examining ascorbate intravenous treatment. Intravenous ascorbate administration can aid in the formation milli-molar concentrations of hydrogen peroxide (H_2O_2), which has pro-oxidant effects and shows a promising ability to kill cancer cells, tartgeting the interstatial fluid that surrounds tumors, without harming normal tissues, neither in blood or tissues [5].

Pharmacological doses of ascorbic acid have been shown to synergize with standard chemotherapy in the treatment of both solid and hematopoietic cancer cells [6]. Inflammations attributed to this process or other possible disease can be ameliorated by vitamin C administrations. Studies also report that the combination of intravenous and oral ascorbic acid treatment further reduces the levels of inflammatory markers, which result to the improvement of the many oncological symptoms [7]. A combination of oral and intravenous ascorbic acid treatment as supportive care is safe, although the literature to date has not supported the efficiency of intravenous vitamin C as monotherapy in anticancer treatment [8].

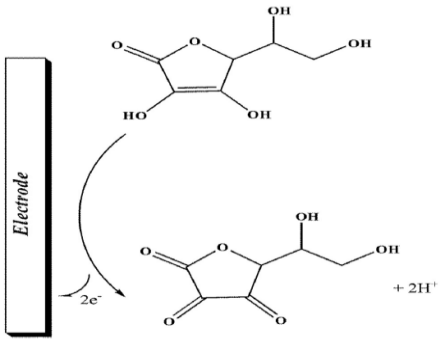

Figure 1.2. Electrochemical mechanism for electro-oxidation of ascorbic acid [9].

A variety of analytical methods, such as conventional titrimetric method, chemiluminiscence, enzymatic methods, fluorimetry, spectrometry, capillary electrophoresis and HPLC have been reported for the detection of ascorbic acid. However, electrochemical methods are of unique interest and represent a promising field for research. For its redox ascorbic acid releases two electrodes and two protons and oxidizes to dehydroascorbic acid [10]. The overall reaction of ascorbic acid oxidation expressed by the following reaction (Fig. 1.2):

$$C_6H_8O_6 \text{ (Ascorbic acid)} \rightarrow C_6H_6O_6 \text{ (Dehydroascorbate)} + 2\ H^+ + 2\ e^- \qquad (1.1)$$

There have been countless scientific studies focused on the deposition of a catalytic paste on an electrode surface, in order to detect electroactive species in a solution of interest. A brief review of catalysts employed to modify the electrode of interest for ascorbic acid detection is documented below.

At a bare Pt electrode in 0.1M KH_2PO solution and in absence of ascorbic acid a cathodic peak was observed, at about -0.1 V, corresponding to reduction of water. However, after the addition of ascorbic acid into the solution, an anodic peak raised around +0.26 V. The return sweeping also showed a reduction peak, associated with water reduction, which shifted to more positive potential in the presence of ascorbic acid, likely related to adsorption of ascorbic acid molecules on the surface of the electrode of interest [11].

Cyclic voltammetry recorded the catalytic activity on sole bare glass carbon electrode and electrode modified with palladium/carbon and cobalt-palladium/carbon catalyst towards the oxidation of 5mM of ascorbic acid in 0.1M phosphate buffer solution, at a pH value of 11, at 20mV s^{-1}. Each of the three of electrodes exhibited electro-catalytic effect on ascorbic acid with oxidation peak potentials at 69 mV, 26 mV and-73 mV respectively. Cobalt-palladium/carbon modified glass carbon electrode turned out to be the most efficient. Co plays a key role for constructing a hybrid system for ascorbic acid oxidation with the reduction of atomic orbital energy and enhancement the electron transfer capability [12].

Cyclic voltammograms of bare electrode in comparison to branch-trunk Ag hierarchical nanostructures/glass carbon electrode in 0.1M PBS, at 4.0 pH (scan rate 50 mVs^{-1}), without ascorbic acid and in the presence 1 mM ascorbic were conducted. In the absence of ascorbic acid, an oxidation peak at 0.295 V, attributed to the self-oxidation of Ag metal was observed, while in the presence of ascorbic acid, a clear oxidation peak was appeared at 0.37 V, clearly owed to the oxidation of ascorbic acid, which illustrated that the self-oxidation of Ag metal had no coupling effect with the reaction of ascorbic acid oxidation. It is also noted that no peaks were shown on the bare glass carbon electrode in the employed potential range. As a result, branch-truck Ag hierarchical nanostructures shown the ability to greatly increase the electro-activity toward the oxidation of ascorbic acid [13].

Cyclic voltammetric responses of the electrochemical oxidation of 0.8 mM ascorbic acid at carbon paste electrode, carbon nanotubes paste electrode, p-aminophenol modified carbon paste electrode and p-aminophenol modified carbon nanotubes paste electrode

were investigated. The oxidation peak potential of ascorbic acid at p-aminophenol modified carbon nanotubes paste electrode alerted by about 290 and 320 mV towards less positive values compared to the carbon nanotubes paste electrode and carbon paste electrode respectively. Oxidation of ascorbic acid at the surface of p-aminophenol modified paste electrode and at p-aminophenol modified carbon nanotubes paste electrode was significantly enhancement[14].

For the determination of ascorbic acid at a 5 mM concentration, carbon nanotubes, manganese nanostructures and manganese nanostructures based carbon nanotubes were tested. Insignificant redox peaks in the cyclic voltammetry at the glass carbon electrode indicate low rate of electron transfer on the surface of the examined electrodes. The addition of manganese nanostructures increased the oxidation peak to about 7.0 μA at 0.6V, attributed to its conductive properties. Compared to bare electrode, manganese nanostructure modified electrode showed an oxidation peak at 0.317 V, indicating the enhancement of electron transfer at the surface of the electro. A further increased peak current of 40 μA with the addition of carbon nanostructures was attributed to their conducting structure, the increase of electroactive surface and fine catalytic properties of manganese when combined with the nanostructures. The higher peak intensity of almost 6 times and the clear oxidation peaks indicate that manganese nanostructures based carbon nanotubes modified electrode contributed significantly to the increase electrochemical activity. Besides, the anodic and cathodic peak potential separation of the modified electrodes was about 200 mV, incident that demonstrates improvement kinetics of electrons at the electrode surface [15].

In the case of chemically reduced graphene oxide sheets modified electrode and graphene sheet /carbon nanotube modified glassy carbon electrode, the oxidation of ascorbic acid showed current peak of 0.222 V, and 0.150 V. As for bare glass carbon electrode, the peak was at 0.666V. Graphene sheet/graphene nanoribbon modified electrode exhibited a low oxidation peak potential at 0.080 V of 176 μA. The shift of -0.03 V towards negative values and the larger current peak illustrated strong electro-catalytic ability of the graphene sheet/graphene nanoribbon modified glass carbon electrode. The increased electroactive surface area and high ability of electric conducting, were contributed to a decreased ascorbic acid oxidation overpotential [10].

The catalytic effect of polyo-methoxyaniline, polyo-methylaniline, and polym-methylaniline hollow spheres in presence of 3 mM ascorbic acid, in citrate/phosphate

buffer solution at 6 pH have been also examined. There was no significant oxidation peak at the bare glass carbon electrode in the experimental potential range. Polym-methylaniline exhibited irreversible oxidation peak at 0.664 V with the peak current at 44.34 mA. The ascorbic acid oxidation peak for the polyo-methoxyaniline showed a similar peak current to the one of the polym-methylaniline. However, it was shifted to more negative potentials at -0.522 V. Finally, an oxidation peak with a higher peak current at 55.16 mA was observed at more negative potential of.-0.391 V, for the polyo-methoxyaniline [16].

Bismuth-silver bimetallic nanoparticles have been deposited at glass carbon electrode for the detection of 0.4 mM ascorbic acid in 0.1 M Phosphate buffer solution at pH 5.0. At the bare glass carbon electrode, the oxidation peak of ascorbic acid occurs at approximately +0.550V (vs. Ag/AgCl), with a relatively broad oxidation peak. For the modified glassy carbon electrode however the case is different, as a sharp oxidation peak at +0.380V was obtained. The sharper peak in conjunction with the significant increase of the anodic peak current revealed that this catalyst enhances the kinetics of the electrochemical process as a very effective promoter. The electrocatalyst layer increases the conductivity, compared to the bare electrode, due to due to the high specific surface area that it establishes. The ascorbic acid molecules can easily pierce through the conductive layer to the electrode, leading to great sensitivity and selectivity [17].

The response of rice starch based nano/mesoporous carbon-modified electrode towards the oxidation of ascorbic acid has been investigated. The peak potential shifted about 300 mV towards negative values, compared to the unmodified glass carbon electrode. The ability of ascorbic acid to transfer its electrons was clearly increased from this electro-catalyst. The irreversible oxidation process of ascorbic acid can be ascribed to the increase of active surface area, pore volume and surface roughness of the electrode surface [18].

In presence of NADH at neutral 7.0 pH, glassy carbon paste electrode has been modified with CdO nanoparticle and 1-methyl-3- butylimidazolium bromide. The current peaks at 0.3 to 0.4 V, with current densities of 150, 200, 250, 300 $\mu A\ cm^{-2}$ for bare carbon paste electrode, CdO/carbon paste electrode, 1-methyl-3-butylimidazolium bromide ionic liquid/carbon paste electrode, CdO nanoparticle/1-methyl-3-butylimidazolium bromide ionic liquid/carbon paste electrode respectively established great catalytic activity of the examined catalyst [19].

NiO nanoparticles and 1-butyl-3-methylimidazolium tetrafluoroborate has been also tested as an active catalyst. Weak electrochemical oxidation peak was observed at carbon paste electrode, compared to one modified with 1-butyl-3-methylimidazolium tetrafluoroborate/NiO nanoparticles/carbon paste electrode, with the oxidation peak current of 163.5 μA over the same conditions. The ascorbic acid oxidation current peak at the bare and at NiO nanoparticles/carbon paste electrode was observed around 960 to 1000 mV with the oxidation current to be at 21.5 and 58.5, respectively. However, at the surface of 1-butyl-3-methylimidazolium tetrafluoroborate/NiO nanoparticles/carbon paste electrode the oxidation peak current was 101.5 μA, value that established great improvement of the electrochemical oxidation response of ascorbic acid in the presence this catalyst [9].

Deposition with reduced graphene oxide-wrapped hierarchical TiO_2 nanocomposite has also been investigated. Cyclic voltammograms recorded on bare glass carbon, TiO_2 modified glass carbon electrode and reduced graphene oxide-wrapped hierarchical TiO_2 modified glass carbon electrode were compared, in 0.1 M PBS, pH 8.0, containing 1 mM ascorbic acid. The bare glass carbon electrode showed no distinct current response in the potential scanning range of –0.2 to 0.2 V, while a direct oxidation peak 0.08 V was observed with the TiO_2 modified electrode, suggesting that TiO_2 particle enhances the electrochemical reaction rate on the electrode surface. Furthermore, reduced graphene oxide-wrapped hierarchical TiO_2 modified glass carbon electrode lowered the oxidation peak potential at 0.02 V and increased current response, which demonstrated that reduced graphene oxide-wrapped hierarchical TiO_2 can further enhance the catalyzed oxidation of ascorbic acid [20].

Majede Bijad studied the effect of ZnO/carbon nanotubes nanocomposite ionic liquid with cyclic voltammetry, using 800 μmol/l ascorbic acid, pH 7.0, with 100 mV s^{-1} scan rate. A relatively low redox activity peak was observed at ZnO/carbon nanotubes/carbon paste electrode and at unmodified electrode, at this potential range. The oxidation peaks potential for ascorbic acid at ZnO/carbon nanotubes/carbon paste electrode and at carbon paste electrode was observed around 670 and 680 mV vs. the Ag/AgCl reference electrode with the oxidation peaks current of 133.0 and 93.5 μA, respectively. ZnO/carbon nanotubes/ionic liquid/carbon paste electrode exhibited significant oxidation peak current around 610 mV with the peak current of 334.1 μA. At the surface of bare carbon paste/ionic liquid electrode, the oxidation peak appeared at 620 mV with the peak current was 265.0 μA. These results indicated its good catalytic activity, with the enhance of peak currents and decrease of the oxidation potential(overpotential) [21].

Finally, the electro-catalytic activity of mesoporous silica encapsulating polyaniline decorated with gold nanoparticles has been used to detect ascorbic acid. Platinum foil was used as counter electrode and Ag/AgCl was used as reference electrodes. PM silica resulted into a peak current of 390 mV, with PGM silica-modified carbon paste electrode also at resulting to 390 mV as well [22].

Table 1-1: Comparison of modified electrodes in the literature.

Working Electrode	**Reference Electrode**	**Concentration Range (mM)**	**Peak Potential (V)**	**Detection Limit (µM)**	**Refs**
DL-Ala/Pt	Ag/AgCl	2-7.5	0.2	9.24	[11]
CoPd/C	Ag/AgCl	0.1-3.42	-0.5	0.1	[12]
branch-trunk Ag	Ag/AgCl	0.17-1.80	0.37	0.06	[13]
APMCNTPE	Ag/AgCl	0.2-12	0.32	0.08	[14]
CNTs-Mn NPs	Ag/AgCl	0.01-0.5	0.6	0.1	[10]
GS/GNR	Ag/AgCl	0-5.0	0.08	0.23	[15]
PmMA	Ag/AgCl	0-3.0	0.39	0.18	[16]
Bi-AgNPs/GCE	Ag/AgCl	0.4-1.2	0.23	0.16	[17]
RSNMC	Ag/AgCl	0.005-6.0	0.3	0.003	[18]
CdO/NP/IL/	Ag/AgCl	0.07–480	0.414	0.03	[19]
BMITB/NiO/NPs	Ag/AgCl/KCl	0.08-380	0.96	0.04	[9]
RGO–TiO2	Ag/AgCl/KCl	1-1500	0.02	0.05	[20]
ZnO/CNTs	Ag/AgCl	0.1–450	0.61	0.07	[21]
PGM silica	Ag/AgCl	0.001-0.75	0.39	0.1	[22]

1.3 Electrochemical detection of uric acid and its importance

Uric acid ($C_5H_4N_4O_3$) is an organic heterocyclic compound (Fig. 1.3) produced in the liver, muscles and intestines. It is the final product of the purine catabolism, deriving from its precursor xanthine, which is degraded by the enzyme xanthine oxidoreductase. Dissimilar to most mammals, humans lack the enzyme that is able to degrade uric acid into allantoin and tend to have much higher uric acid levels, which is linked to a constellation of clinical conditions and diseases, such as the commonly known gout. However, these higher concentrations in humans also enhance their survival advantage, as hyperuricemia maintains better blood pressure in the face of low dietary salt [23].

Uric acid is considered to be one of the most important antioxidants in the blood and central nervous system. These antioxidant properties results into neuroprotective effects, as uric acid scavenges free radicals in the blood [24].

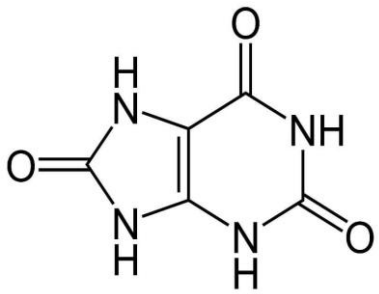

Figure 1.3. Chemical structure of uric acid [25].

High uric acid concentrations have been reported in many systemic diseases, such cardiovascular diseases, metabolic syndrome and hyperuricosuria [26]. High levels of uric acid have also been noted in peripheral neuropathies, such as diabetic sensorimotor polyneuropathy [27] and chronic inflammatory demyelinating polyneuropathy [28]. In multiple sclerosis and amyotrophic lateral sclerosis however, low levels have been reported and uric acid decreases further as the disease progresses [29].

Nevertheless, there are indications that uric acid also has health promoting and disease preventing qualities. Regulation of uric acid and its precursors' concentration is an effective way to prevent or treat certain conditions. Higher uric acid has been associated with a reduced risk of developing neurological disorders, such as Parkinson's disease [30], as well as increase bone density that decreases the chance of osteoporosis [31].

The electrochemical oxidation of uric acid has been investigated under many different conditions such as pH, temperature and molarity. Uric acid undergoes a two-electron oxidation reaction (Fig. 1.4), which leads to the formation of an unstable anionic quinoid compound. If the pH is greater than 6 then it also undergoes two nucleophilic addition of water to the quinoid form, followed by a final decomposition reaction, which results into allantoin, the final product [32].

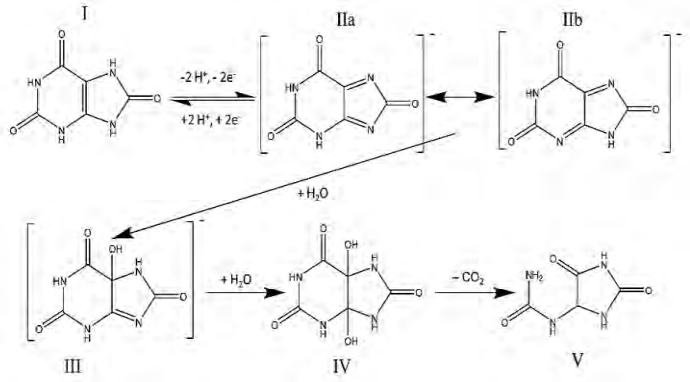

Figure 1.4. Oxidation of uric acid to allantoin [32].

For uric acid determination, an early work constructed a Pt/Au hybrid film electrode showed efficient electro-catalytic functions not only towards the oxidation of uric acid but also in simultaneous determination of dopamine, ascorbic and uric acid in a mixture. Regarding uric acid, the bare electrode resulted into an oxidation at 0.54 V, compared to the oxidation at the Pt/Au hybrid film, which occurred at 0.52 V. This observed shift of the oxidation potential and increase of current peak demonstrated that the examined catalyst has good catalytic activity. Oxidation currents are also increased at a stable rate with the rise of concentration levels of these compounds [33].

The voltammetric responses of the bare glass carbon electrode and single-walled carbon nanohorn modified glassy carbon electrode towards uric acid was examined. A reversible

redox pair for uric acid was exhibited at the single-walled carbon nanohorn modified glassy carbon electrode with the separation of anodic and cathodic peak to be at 31 mV. The anodic peak current was notably enhanced, indicating the good catalytic ability of this electro-catalyst for uric acid oxidation. The results also demonstrate that single-walled carbon nanohorn can accelerate the oxidation [34].

In another study, the cyclic voltammograms of bare glassy carbon electrode, graphene and graphene/Pt nanocomposite electrodes were measured in 1 mM uric acid solution. The anodic peak currents were 102 μA for glass carbon electrode, 183 μA for graphene and 371 μA graphene/Pt modified electrode. Both graphene and graphene/Pt modified electrodes enhanced the electrochemical sensing and indicated that the Pt nanoparticles suitable for uric acid sensing. However, the oxidation currents for uric acid were not increased with a high Pt/graphene ratio [35].

It has also been found that graphene decorated with gold nanoparticles modified glassy carbon electrode exhibits excellent electro-oxidative properties for uric acid in 0.10 M NaH_2PO_4–HCl buffer solution at 2.0 pH. Good linear relationships were observed, indicating that uric acid was indeed electro-active under diffusion controlled processes for the examined catalyst. The oxidation of uric acid was also found to be irreversible [36].

Pt and Pd ions have been employed to fabricate PdPt/polydiallyldimethylammonium chloride-reduced graphene oxide nanomaterials to modify a glassy carbon electrode, in order to detect uric acid. The voltammetric peaks obtained by differential pulse voltammetry measurements were 18 μA and 0.27 V. For the 4-400 μM range tested, the catalyst displayed good electro-catalytic activity towards the oxidation of uric acid. The proposed sensor could be also successfully utilized for the detection of uric acid in human blood serum and human urine samples. It has been also successfully applied to determine uric acid in human urine. On polydiallyldimethylammonium chloride-reduced graphene oxide/glass carbon electrode, the redox peak currents increased, apparently due to good electrical conductivity and high surface to volume ratio of the reduced graphene electrode. The peak currents increased in both modification of the glass carbon electrode with Pt/polydiallyldimethylammonium chloride-reduced graphene oxide and

Pd/polydiallyldimethylammonium chloride-reduced graphene oxide nanomaterials, possibly attributed to the properties of reduced graphene oxide metal nanoparticles, which boost the transfer of electrons at the electrode surface. In addition, the redox peak currents increased at Pd3Pt1/ polydiallyldimethylammonium chloride-reduced graphene oxide/glass carbon electrode with the peak-to-peak separation as 81 μA, which was higher than those of the previous catalysts, indicating that Pd_3Pt_1/ polydiallyldimethylammonium chloride-reduced graphene oxide/glass carbon electrode nanocomposites promotes the catalytic activity and electric conductivity at the best possible way [37].

More recently, a uric acid electrochemical sensor was constructed with cationic polydiallyldimethylammonium chloride functionalized reduced graphene oxide and anionic au nanoparticles mixed with polyoxometalates clusters $K_8P_2W_{16}V_2O_{62}$ ($P_2W_{16}V_2$-Au). The oxidation peak current of uric acid was found to be 103 μA, with the oxidation peak potential at 0.35 V. The proposed sensor achieved good performance, as well as stability, reproducibility and selectivity, qualities that ensures the electrochemical sensor suitability for uric acid determination [38].

In 2017 a cubic Pd and reduced graphene oxide modified glassy carbon electrode was fabricated to detect uric acid alone or simultaneously with dopamine. Focusing on uric acid, the oxidation peak current was reached 115μA, while the peak potential reached 0.316 V, establishing the feasibility of uric acid detection in rat urine and serum samples. The oxidation peak current on Pd/reduced graphene oxide/glass carbon electrode was increased at 124.8 μA. The results indicated that this catalyst has good electrocatalytic activity towards uric acid. The synergy of both Pd nanocubes and wrinkled reduced graphene oxide promoted this property, as the unique cubic Pd/reduced graphene oxide structure has many active sides, while the great conductivity of reduced graphene oxide boosted the transfer of electrons between at the catalyst surface [39].

In the same year a sensitive and selective electrochemical sensor based on 3D graphene hydrogeld/gold nanoparticles nanocomposite for detection of uric acid was successfully developed. The peak values were observed at 30μA, 0.32 V. Under optimum conditions, the 3D graphene hydrogel/gold nanoparticles nanocomposite/glassy carbon electrode exhibited linear responses to uric acid oxidation in a ranges for 1 to 60 μM [40].

A hierarchical nanoporous PtCu alloy in order to electrochemically determine uric acid was also fabricated. The sensor exhibited high electrochemical activity towards the oxidation of the compound at 0.61 V, displaying a wide linear response in the range of 10 to 70 μM [41], while Wu *et al.* [42] proposed a Pt–Ni/multiwalled. The catalyst presented good electro-catalytic activity and provided a long linear range from 0.1 to 240.4 μM, while also exhibited great selectivity, stability and reproducibility. The anodic peaks were approximately at 0.3 V and the peak currents of the Pt–Ni/multiwalled carbon nanotubes were substantially larger than that of the Pt–Ni/carbon black, suggesting that Pt–Ni/multiwalled carbon nanotubes are the most suitable for detection. The increase of the concentration resulted in increase of the anodic peak current al well, indicating its sensitivity, while no oxidation peak was present in the absence of uric acid.

Table 1-2: Comparison of modified electrodes in the literature.

Working Electrode	Reference Electrode	Concetration Range (μM)	Peak Potential (V)	Detection Limit (μM)	Refs
PtAu/GCE	Ag/AgCl	21-336	0.52	21	[33]
SWCNH/ GCE	Ag/AgCl	0.06-10	0.359	0.02	[34]
Pt-Graphene/GCE	Ag/AgCl	0.05-11.85	0.387	0.05	[35]
AuNPs-β-CD-Gra/GCE	SCE	0.5-60	0.55	0.21	[36]
PdPt/PDDA-RGO/GCE	SCE	4-400	0.27	0.1	[37]
[P2W16V2-Au/PDDA-rGO]	Ag/AgCl	0.25-150	0.35	0.08	[38]
Cubic Pd/RGO/GCE	SCE	4-469.5	0.316	1.6	[39]
3DGH-AuNPs/GCE	Ag/AgCl	1.0-60	0.32	0.01	[40]
hnp-PtCu	RHE	10.0-70	0.61	5.7	[41]
Pt–Ni/MWCNT	SCE	0.1-240.4	0.3	0.03	[42]

CHAPTER 2: Electrochemical devices

2.1 Fuel Cell

A fuel cell is an electrochemical device that converts chemical energy from a fuel to electricity, through the electrochemical reaction of the fuel with oxygen or another oxidizing agent. It is consisted by an anode, a cathode and an electrolyte that allows the movement of positively charged hydrogen ions, protons, between the two sides of the fuel cell. At the anode a catalyst causes the fuel, which is most commonly hydrogen, to undergo oxidation, which produces protons and electrons [43].

In general, the anode of any two-port device, like a diode or resistor, is the electrode where electrons flow out. The protons move from the anode to the cathode through the electrolyte, after the reaction occurs. In parallel electrons are drawn from the cathode to the anode through an external circuit, generating a direct electrical current. At the anode, the electrode where electrons flow in, is also a catalyst that causes electrons and oxygen to react with the protons, forming water [44].

In addition to electricity and water, fuel cells generate heat and may produce emissions, such as very small amounts of nitrogen dioxide and carbon dioxide, depending on the selected fuel. It should be also noted that the electrolyte must only allow protons to pass through and not electrons in any case, otherwise the electrons would go through the electrolyte and not through the external circuit, which would result in their loss and not sufficient use.

In a typical hydrogen fuel cell, the reaction is split into two electrochemical half reactions:

$$H_2 \rightleftharpoons 2H^+ + 2e^- \quad (2.1)$$

$$O_2 + 2H^+ + 2e^- \rightleftharpoons H_2O \quad (2.2)$$

Nonetheless, there are many types of fuel cells, such as phosphoric acid, polymer electrolyte membrane, alkaline, molten carbonate and solid-oxide. For example, a phosphoric acid fuel cell includes a liquid H3PO4 electrolyte contained in a thin SiC matrix between two porous graphite electrodes coated with a platinum catalyst (Fig. 2.1). The H_3PO_4 electrolyte can be either pure or just highly concentrated. Hydrogen is used as the fuel, while oxygen, or even the surrounding air can be used as oxidant. The anode and cathode reactions are respectively:

$$\text{Anode: } H_2 \rightarrow 2H^+ + 2e^- \tag{2.3}$$

$$\text{Cathode: } ½\ O2 + 2H^+ + 2e^- \rightarrow H_2O \tag{2.4}$$

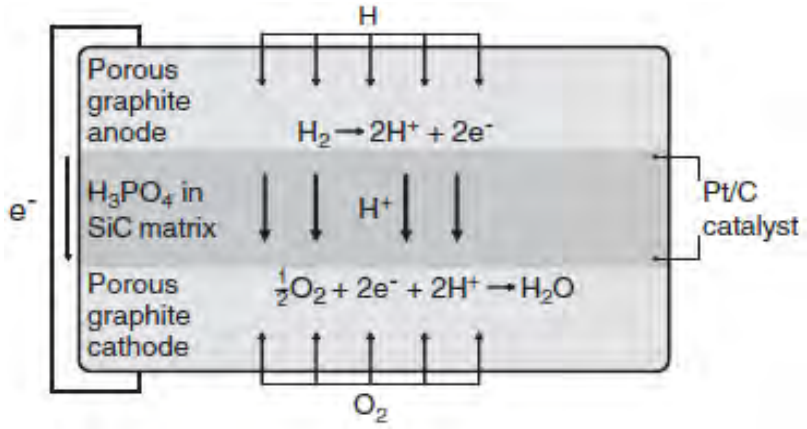

Figure 2.1. A typical phosphoric acid fuel cell representation [44].

Essentially, fuel cells have various advantages compared to other power sources. They are generally more efficient than combustion engines, whether piston or turbine based and since there is no combustion, fuel is converted to electricity more efficient.

The essential elements of a fuel cell are stable, with none or only few moving parts, which leads to highly reliable and sustainable. In addition, specifically in the case of hydrogen fuel cells, the by-product of the main fuel cell reaction can be pure water, theoretically

zeroing emissions, one of the main advantages of fuel cells when used in vehicles, as there is an urgent need to reduce vehicle emissions, especially within cities.

2.2 Batteries

A battery consists of an anode, a cathode, an electrolyte, a separator and the external case. The main difference between battery and fuel cell systems is that fuel require fuel from an outside source, while the battery as a closed system does not. Another difference is the materials used as electrodes and electrolyte, which determines the specific characteristics of the systems. Separators are composed of polymeric materials, paper or paperboard, while the external case is made of steel, polymeric materials or paperboard. In general, electrodes and electrolytes change on the different applications of batteries [45].

As far as household use there are two basic types of batteries, which are the single use, primary cells and the rechargeable, secondary cells. Among primary cells, the most used are the alkaline-manganese and the zinc-carbon. Alkaline-manganese batteries are composed of a brass rod in contact with powdered zinc as anode and a steel case in contact with carbon and MnO_2 as cathode (Fig. 2.2), while A paste of KOH is used as alkaline electrolyte. Zinc-carbon batteries typically have a carbon rod in contact with carbon and MnO_2 as cathode and a zinc case as anode. A paste of NH_4Cl and $ZnCl_2$ is utilized as electrolyte. The cylindrical cell the zinc electrode is recovered with a stainless steel jacket, while a plastic or paperboard separator and an asphalt seal are usually included.

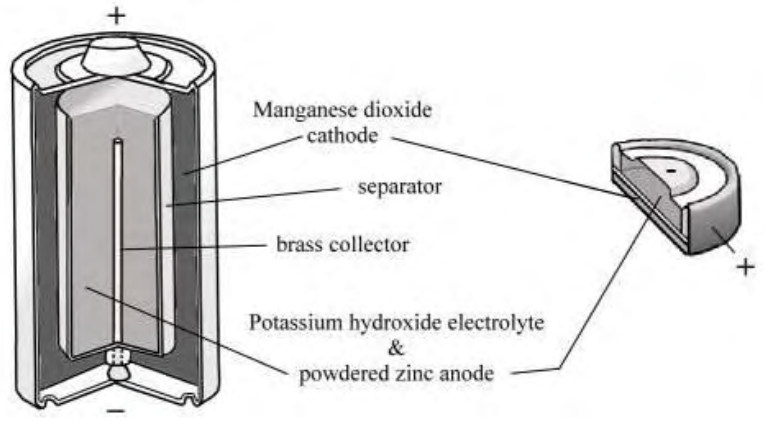

Figure 2.2. A conventional battery consisted by a manganese dioxide cathode, a powdered zinc anode and a potassium hydroxide electrolyte [46].

One of the most hazardous systems in terms of disposal was NiCd, commercially used since 1950. The anode consists NiOH and the electrolyte is usually a mixture of $LiOH_2$ and KOH [47]. Lithium on the other hand, contained no toxic metals and as the lightest of the other used metals provides the largest energy content, providing great electrochemical potential. However, there is a possibility of fire immerging if the metallic lithium is exposed to moisture while the cells are corroding. These batteries must be fully discharged in order to consume all metallic lithium content.

The first step in tapping the actual potential of Li-ion began in 1912 by G.N Lewis, but it was not until the early 1970's that the first lithium ion non-rechargeable batteries were made commercially available. These batteries were made with TiS_2 as cathode and Li metal as the anode [48]. In the 1990s the new rechargeable Li-ion battery was put on the market. Li ion battery technology is based on the fact that lithium, is also the most electropositive metallic element and. This battery type has been found to be stable at over 500 cycles, can be fabricated in different shapes and sizes and require very little maintenance compared to the other batteries, while researcher work towards the improvement the cycling life, increase the safety and decrease the manufacturing cost. Li ion batteries are used in high-end electronics, have recently been introduced to the power tool markets and they are entering the hybrid electric vehicle market, making it a serious contender for powering the electric cars of the future [49].

Conserving lithium batteries there is an important difference between the primary and secondary batteries. Primary cells use metallic lithium as cathode, while rechargeable batteries use a material like $LiXMA_2$ at the positive electrode and graphite at the negative electrode. Some materials used at the cathode include $LiCoO_2$, $LiNiO_2$ and $LiMn_2O_4$. The electrolyte can be an organic liquid with dissolved substances like $LiClO_4$, $LiBF_4$ and $LiPF_6$ [50].

Nickel metal hydride (NiMH) batteries were developed in 1989 and commercialized in 1990, primarily in Japan. NiMH batteries have high electrochemical capacity and good environmental compatibility. They function efficiently within a wide range of temperatures, within −20 to 60 ◦C and possess wide lifespan of 500 to 1000 cycles. The positive electrode comprises porous Ni plate with nickel hydroxide as the activating agent. The negative electrodes consist of a hydrogen storage alloy powder, such as Ni–Co or other miscellaneous metal on a metal-mesh substrate, while an inert insulating layer separates the two electrodes. As for the electrolyte, usually potassium hydroxide is used. NiMH batteries are considered environmental friendly and could replace NiCd batteries in many applications. However, comparted to NiCd batteries, the costs of production are considerably higher [51].

Among the different types of batteries there is one type that shows unique potential, the metal-air battery. This type of battery uses oxygen from the ambient air as active material at one of its electrodes. Since the active material does not need to be kept inside the battery, almost the entire space inside the battery can be utilized for the active material of the other electrode. This results to higher capacities, both by weight and by volume, at batteries with air electrodes. However, the other electrode materials need to meet certain requirements in order to be able to take advantage of the free space. Promising candidates include zinc, aluminum, lithium and iron [52].

Zinc air batteries are a promising battery technology, which takes advantage of the use of the presence of oxygen in the air as a source of oxidizing agent. They have significantly higher energy density comparing to other batteries for this reason. Where normally a solid fuel would be required, zinc air batteries use of the oxygen in the air substantially reduce the mass and the volume of the battery required. Based on mass energy density zinc air

batteries can reach two or three times the energy density of the currently used lithium ion batteries. Correspondingly a significant development in volumetric energy density can be achieved, as zinc air batteries has the potential for improvements by as much as 50%.

The high electro-positivity, environmentally benignity and low cost of zinc makes it an excellent material for use in energy storage. Zinc air batteries have two electrodes, one solid zinc electrode, which functions primarily as the anode during discharge and one air breathing electrode, which allows the diffusion of air into the cell. To prevent particulate transfer from one electrode to the other, the electrodes are separated by a separator membrane. The membrane can also be treated to prevent zinc ion and zinc hydroxide transfer to the cathode of the cell, which can result to short circuiting in cells which undergo a considerable amount of cycling [53].

Aluminum as an anode is appealing for a number of reasons. It has the ability to transfer three electrons per atom, has low atomic mass and high negative standard potential. These characteristics lead to a high theoretical energy density. In addition, there is large abundance in nature and low production of aluminum. In an al-air battery all the fuel is stored in the anode [54]. It can also be discharged in saline, a mixture of sodium chloride in water, acidic and alkaline electrolytes. However, due to the higher conductivity and solubility of alkaline electrolytes, al-air systems have an advantage over saline systems. Aluminum suffers substantial corrosion in alkaline solution, which results in fuel loss during standby and coulombic losses on discharge [55].

Due to their high theoretical energy densities li-air batteries are considered as one of the most important battery systems, which contribute towards a number of applications. Li-air batteries are different from many primary and secondary batteries, as the active materials are a pure lithium metal as the anode material and oxygen from surrounding air is not stored inside the cell, but can continuously be derived from the environment around the cell. The use of ambient air as the active oxidant makes Li-air battery safer than commercial lithium-ion batteries. Li-air batteries have received much attention, because they provide a superior theoretical specific energy about 5-10 times better than conventional rechargeable Li-ion batteries, using $LiMn_2O_4$ or $LiCoO_2$ as the positive

electrode [56]. However, low current density, low charge-discharge efficiency and inadequate cyclability are limiting factors for the performance of Li-air batteries. All of these problems are primarily due to the pore structure of the air electrode and interfacial reactions of oxygen with the li-ions. In addition to these problems, the discharge li-air reaction is affected by the insoluble lithium oxides discharge products, which can cover the active surface area of the cathode and block the pathway for other reactive species, preventing further reactions inside the cathode. It should be also noted here that batteries using cathodes with cobalt and nickel present risk to health and have negative environmental impact. This is a result of the production, processing and usage of these heavy metals leading to ecological hazards on disposal and progressively global warming. Researches seek to develop innovative components in the li-air cell, such as new materials for the positive electrode, electrolyte and catalyst to address these issues [57].

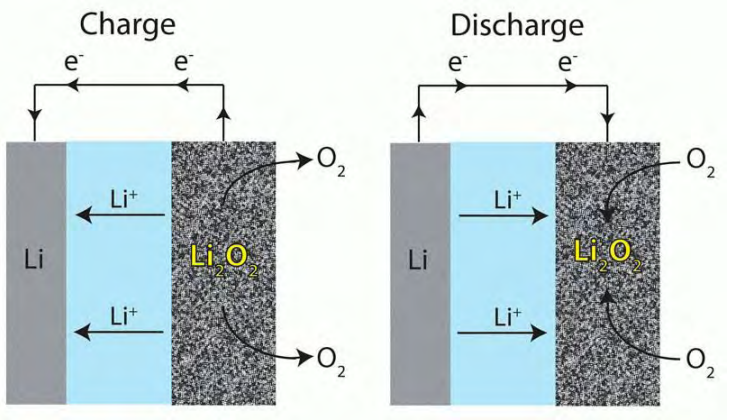

Figure 2.3: Li-air battery charge and discharge scheme [58].

Although lithium-air batteries have showed extremely high discharge capacity, the supply of lithium is not abundant and may run out in the foreseeable future. Sodium on the other hand, is the fourth most abundant element in the earth and thus provides potential to be an alternative source to lithium. It is an element with wide availability and low cost, aspects that make it a promising material for energy storage systems application [59]. The reaction mechanism of sodium is similar to lithium, hence making it possible to replace the anode materials without changing the configuration of the system. Since the discharge products of sodium-air batteries are not soluble in the organic electrolyte, but they are been deposited on the electrode similarly

to lithium-air batteries, the cathode materials and structures can significantly impact the battery performance [60].

2.3 Supercapacitors

Electrochemical supercapacitors, or ultracapacitors have attracted the attention of researchers, due to their high power density and long lifecycle. They combine the high power output of traditional dielectric capacitors and the high energy storage of fuel cells and batteries [61].

A function of an electrochemical supercapacitor is be to boost the battery or fuel cell in a hybrid electric vehicle to provide the necessary power for acceleration. Another function is is to recuperate brake energy. Electrochemical supercapacitors could play an important role future energy storage functions, by providing powerful back-up supplies against power disruptions [62].

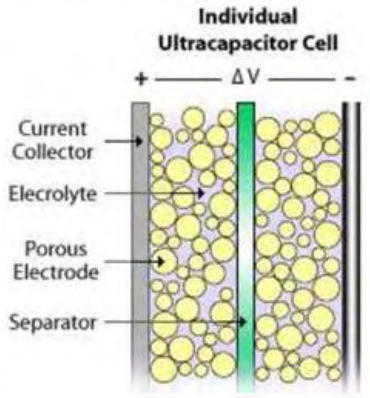

Figure 2.4. An ultracapacitor cell representation [63].

An electrochemical supercapacitor is an energy-storage device, similar to batteries in manufacturing and design. It is consisted of two electrodes, an electrolyte and a separator that electrically isolates the two electrodes. The most important component in an electrochemical supercapacitor is the material of the electrode. They are fabricated from nanoscale materials that have high porosity and high surface area. Energy can be stored at the interface between the conductive solid particles, such as carbon particles or metal oxide

particles and the electrolyte. This interface can be considered as a capacitor with an electrical double-layer capacitance.

A main type of electrochemical supercapacitors is the electrostatic supercapacitor, at which the electrode material is not electrochemically active and no electrochemical reaction on the electrode material during the charging and discharging processes. The charge accumulation occurs at the electrode electrolyte interface. Another main type is the faradaic supercapacitor, at which the electrode material is electrochemically active and can directly store energy during the charging and discharging processes [64].

One of the most important supercapacitor components is the electrolyte, which resides inside the separator and the active material layers. An effective and sufficient electrolyte in supercapacitors has a combination of properties, including ionic concentration at a high rate, high electrochemical stability, wide voltage window, low resistivity, low viscosity, low volatility, low toxicity, low cost and high purity. The electrolytes used can be classified into three types: aqueous electrolytes, organic electrolytes and the ionic liquids.

Aqueous electrolytes, such as H_2SO_4, KOH, Na_2SO_4 and NH_4Cl aqueous solution and many other, can provide a higher ionic concentration and lower resistance than organic electrolytes. In addition, due to higher ionic concentration and smaller ionic radius, supercapacitors that contain aqueous electrolyte may display higher power and capacitance than those with organic ones. Also, in contrast with an organic electrolyte, which needs strict conditions and processes to obtain highly pure electrolytes, the preparation and utility of aqueous electrolytes can be engineered without extreme preparation and conditional control. Unfortunately, the small voltage window(1.2V) of aqueous electrolytes is a major disadvantage, which limits the possible improvement in both power and energy densities. This is the reason why organic electrolytes are mostly recommended.

Compared to aqueous electrolytes, organic electrolytes can provide a wider voltage window. Among many organic electrolytes, acetonitrile and propylene carbonate are the most commonly used solvents. Compared to other solvents, acetonitrile can dissolve big amounts of salt, but may cause toxic and environmental problems. Propylene carbonate electrolytes offer a broad range of operating temperatures, a wide electrochemical window

and good conductivity, while being friendly to the environment. Organic salts such as triethylmethylammonium tetrafluoroborate and tetraethylphosphonium tetrafluoroborate are also been used in supercapacitor electrolytes. Less symmetric salts have increased solubility and lower crystal-lattice energy. However, an organic electrolyte must maintain high purity. A water content over 3–5 ppm can significantly reduce its voltage.

Ionic Liquids can exist in liquid form at a verity of desired temperature. Their exceptional properties, such as high chemical and thermal stability, low vapor pressure, low flammability and wide electrochemical stability window sets them excellent candidates for supercapacitor electrolytes. The main liquids studied for supercapacitor applications are pyrrolidinium, imidazolium and asymmetric, aliphatic quaternary ammonium salts with anions such as tetrafluoroborate, bis(trifluoromethanesulfonyl)imide, trifluoromethanesulfonate, bis(fluorosulfonyl)imide and hexafluorophosphate [65].

The electrical double-layer capacitance comes from electrode material particles, such as the interface between the electrolyte and the carbon particle. A deficit or an excess of electric charges is accumulated on the electrode surfaces and charged electrolyte ions are built up on the electrolyte side in order to preserve electroneutrality. Within the electrolyte cations move towards the negative electrode while anions move towards the positive electrode. During discharge, the reverse process takes place. Throughout the process, charge transfers across the electrode and the electrolyte interface and net ion exchanges between the electrode and the electrolyte do not occur, which mean that the electrolyte throughout the whole process remains constant [66].

Faradaic supercapacitors, or pseudo-capacitors exhibits significant larger capacitance values and energy density than an electrostatic supercapacitor, because its electrochemical processes occur both on the surface and in the bulk near the surface of the solid electrode. The capacitance of a faradaic supercapacitor could be 10–100 times higher than the electrostatic capacitance of an electrostatic supercapacitor. However, since faradaic processes are normally slower than non-faradaic processes, a faradaic supercapacitors usually suffers from relatively lower power density than an electrostatic supercapacitor. Furthermore, because redox reactions occur at the electrode, similarly to batteries, a faradaic supercapacitor often lacks stability

during cycling [67]. When a potential is applied to a faradaic supercapacitor, rapid and reversible redox reactions take place on the electrodes, resulting in faradaic current passing through the supercapacitor cell. Electrode materials undergoing such redox reactions include metal oxides and conducting polymers, including RuO_2, MnO_2, and Co_3O_4 [68, 69].

A hybrid electrochemical supercapacitor uses both the electrical double-layer and faradaic mechanisms to store charges. A device can be regarded as hybrid electrostatic capacitors if it has one electrostatic or pseudo-capacitive electrode combined with a rechargeable battery-type electrode. Hybrid electrochemical supercapacitors devices can be based on electrodes based on both pseudo-capacitive materials and electrostatic capacitive materials with different types of structure and symmetry [70].

2.4 Electrolyzers

Electrolysis is an electrochemical process for splitting water into its components, hydrogen and oxygen. The history of water electrolysis dates back to the 1800s when Nicholson and Carlisle discovered the electric water splitting. Although, not before a century from that stage was the first electrolysis technology commercially developed. A basic water electrolysis unit consists of an anode, a cathode, a power supply and an electrolyte. A direct current must be applied in order to keep the electricity balance and the flow of electrons from the negative terminal of the direct current source to the cathode, where the electrons are consumed by hydrogen ions protons to form hydrogen.

In order to keep the electrical charge in balance, hydroxide ions transfer through the electrolyte solution to the anode, at which the ions give away electrons, returning to the positive terminal of the direct current source. For the purpose of enhancing the conductivity of the solution, electrolytes are applied in the electrolyzer, which generally consist of high mobility ions, such as potassium hydroxide and nickel.

Potassium hydroxide is one of the most commonly used in water electrolysis, as it contributes in avoiding the huge corrosion loss, caused by acid electrolytes. Nickel is also a

popular electrode material, due to its good activity and availability, along with low cost. During the process of water electrolysis, hydrogen ions move to the cathode and hydroxide ions move towards the anode. With the use of a diaphragm, gas receivers collect hydrogen and oxygen, which form on the cathode and depart from the anode [71].

The half reactions occurring on the cathode and anode respectively can be written as:

$$\text{Cathode : } 2H^+ + 2e^- \rightarrow H_2 \qquad (2.5)$$

$$\text{Anode : } 2OH^- \rightarrow \tfrac{1}{2} O_2 + H_2O + 2e^- \qquad (2.7)$$

The electrolyzers that attract the most interest for hydrogen generation are alkaline, polymer exchange membrane and solid oxide. Alkaline electrolysis is the only commercially available technology up to this date. For each electrolyzer cell there are two electrodes, one positive and one negative and an electrolyte interceding in between. The most common metals used in alkaline electrolyzers are Fe, Co, Ni and Pt/C, while the electrolyte is liquefied KOH. The two electrolyzer chambers are divided by a diaphragm. However, this technology produces hydrogen with the lowest purity.

Polymer exchange membrane electrolyzers can be considered as an incremental development of alkaline electrolyzers. Polymer exchange membrane electrolyzers or solid polymer electrolyzers, as they are also called, are based on the reversed polymer exchange membrane fuel cell technology. They operate at the same or higher temperature than alkaline electrolyzers and generally have superior efficiency. The main difference is that they use a more advanced and complex diaphragm. They are about to become commercially available in the near future.

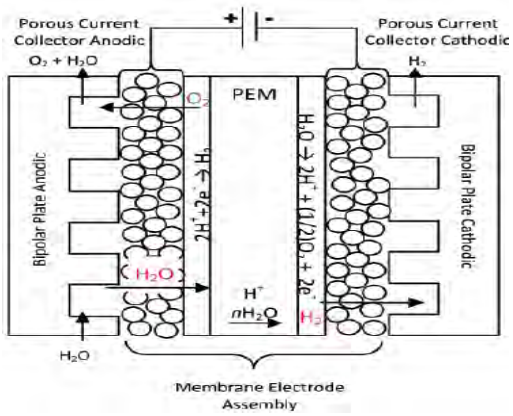

Figure 2.5. Basic schematic of a polymer exchange membrane electrolyzer cell [72].

Solid oxide electrolyzers operate at much higher temperatures than the other technologies and consume much less electricity due to greater energy conversion efficiency. However, due to the high operation temperature, tailored materials are required to withstand the extreme conditions of the process. Solid oxide electrolyzers besides providing the highest faradic efficiency also offer a possibility of direct electrolyzing of CO_2 and can extend to co-electrolyzing H_2O and CO_2 simultaneously. The product of such co-electrolysis is syngas, which can be reprocessed to yield synthetic fuel [73]. However, they are the least commercially developed technology.

2.5 Electrochemical sensors

Electrochemical sensors are based on electrochemical cells of two or three electrode, which are connected with a solid or liquid electrolyte. Each liquid interacts in a different way with the electrochemical cell and produce a specific signal from the measurement of current, potential and electric conductivity changes. Based upon these aspects electrochemical sensors can be divided into three categories: amperometric, potentiometric and conductometric.

2.5.1 Fundamental properties

A chemical sensor is a device that converts chemical information into a measurable signal, providing a certain type of response directly related to the quantity of specific chemical species. Fundamentally, all chemical sensors consist of a transducer, which transforms the response received, into a detectable signal to an appropriate device and a chemically selective layer, which isolates the response of the analyte from the reaction environment.

Sensors can be classified as electrical, optical, mass and thermal sensors and are designed to detect an analyte in the gaseous, liquid or solid state. Chemical sensors contain two basic components, connected in series, a receptor, which is the chemical recognition system and a chemical transducer. There is a diversity of recognition elements and signal transducers.

Electrochemical sensors are an important subdivision of chemical sensors. It is the technology that connects electricity and chemistry, by measuring electrical quantities, such as potential, current and electrical charge and. Electrochemical sensors operate by reacting with the fluid of interest and producing an electrical signal proportional to the fluid's concentration. They are appealing as sensors, due to their experimental simplicity, noteworthy ability of detection and rather low cost. Electrochemical sensors have a wide range of applications in clinical, industrial and environmental fields.

The first electrochemical sensors were manufactured within the 1950s, mainly for oxygen monitoring. In the 1960s the pH glass electrode was the most extensively used sensors [74]. In addition, in 1962, L. Clark Jr. introduced the amperometric glucose enzyme electrode. Thus far, there has been a splendid evolution of accurate sensing devices, based on different transduction and recognition elements.

Electrochemical sensors must meet certain requirements, in order to be considered practical and applicable. Reproducibility is one of the most important aspects. Reproducibility is a measure of the drift in a series of results taken over a period of time. These observations should not greatly differ from one another. The stability of the sensor is also of great significance. The stability may vary, depending on method of preparation of the sensor, its geometry, along with the applied receptor and transducer and the limiting current

response rate. Furthermore, it may vary depending on the operational conditions, such as the analyte concentration, pH and presence of organic solvents.

Electrochemical sensors are insignificantly affected by pressure changes. Nevertheless, keeping the entire sensor within the same pressure is of great importance, since continuously different applied pressure can damage the sensor. However, they are sensitive to temperature change, thus it is beneficial to maintain the sample temperature as stable as possible. Depending on the type of sensor and manufacturer, if the temperature is above 25°C, the sensor will produce slightly higher results. In contrast, the sensor will apprehend lower results, when below 25^{o}C. The temperature effect is typically 0.5% to 1.0% per degree centigrade. The life expectancy of an electrochemical sensor relies on several factors, including the applied fluid of detection and the condition they are used, ideally ranging from one to three or more years, depended by the total amount of measurement and the applied conditions, such pressure, temperature and humidity.

A typical electrochemical sensor is consisted by the sensing, which is referred to as working electrode, a reference electrode and a counter/auxiliary electrode separated by a thin layer of electrolyte. The selection of the electrode material is crucial as it catalyzes the half-cell reaction over functioning time. All three electrodes can be made of different materials in order to complete the cell reaction. Typically, the electrode is made from a noble metal, such as platinum or gold, while the reference electrode can be composed by Ag/AgCl or Hg/Hg2Cl2. The counter electrode is usually of conducting material, such as platinum and graphite.

The working electrode is where the reaction of interest occurs. Consequently, it is important to have a stable and constant potential at this certain electrode. However, the sensing electrode’s potential cannot remain stable, due to the continuous electrochemical reactions that take place on its surface, causing deterioration of the performance over extended periods of time. This is the reason the reference electrode is introduced. The reference electrode is placed within the electrolyte, in close proximity to the working electrode. The reference electrode maintains the value of the fixed stable voltage applied at the working electrode, while no current flows to or from the reference electrode.

There is a variety of electrodes, mainly divided to liquid and solid electrodes. Liquid–membrane electrodes are widely used for potentiometric measurements. They are based on liquid substances that cannot be mixed with water, permeated in a polymeric membrane, which is used to separate the targeted solution from the inner compartment that contains the target ions. The membrane–active recognition can be accomplished by a liquid ion exchanger [75] or by a neutral macrocyclic compound, having molecule–sized dimensions containing cavities to surround the target ions [76].

Ion-selective electrodes membrane-based potentiometric electrodes are capable of accurately measuring the activity of ions in solution. They can be prepared with crystalline, liquid and polymer membranes, allowing for the selective measurement of a wide variety of cations and anions. Depending on the nature and composition of the membrane materials used to fabricate the electrode, selectivity for one ion over another can be achieved [77].

In halfway of the 1970 decade, Freiser introduced coated-wire electrodes [78]. A conductor is directly coated with an appropriate ion-selective polymer membrane, wither a polyvinyl chloride, polyvinylbenzyl chloride or polyacrylic acid, in order to obtain a sensitive electrode to electrolyte concentrations. Their response is similar to that of the classic ion selective electrodes, with regard to detectability and range of concentration [79].

Solid electrodes are prevalent as electrode materials, due to their versatile potential range, low background current, chemical idleness, eligibility for numerous sensing applications and low cost. They can be fabricated by carbon, gold, silver, platinum, copper, nickel and copper. The solid electrodes exhibit major advantages as they can easily be miniaturized, fabricated in the form of disposable sensors, have enhanced mechanical robustness, their dimensions are suitable for both, in vitro and in vivo measurements and their preparation is relatively simple and low cost [80].

A modern approach to solid electrode systems is the development of chemically modified electrodes, where modification of the electrode’s surface is introduced with an appropriate surface modifier. Chemically modified electrodes result from the immobilization of a modifier agent onto the electrode surface, though chemical reactions, polymer coating, absorption and composite formation. Compared to conventional electrodes, they show

enhanced physicochemical characteristics. The immobilization of chemical microstructures onto electrode surfaces has been a primary development area in electrochemistry.

An electrolyte is a key factor to the elimination of electron migration effects, the reduction of solution's inert resistance and the maintenance the ionic strength constant. The electrolyte facilitates the cell reaction and carries the ionic charge across the electrodes, while forming a stable reference potential with the reference electrode. Choosing the suitable electrolyte components and arranging their geometry is important to determine the optimum operating performance.

Minor variations can have a major effect on the sensor's accuracy, selectivity, sensitivity, response time and life expectancy. For example, if it evaporates rapidly, the signal of the sensor will deteriorate. As compared to liquid electrolytes, solid electrolyte sensors demonstrate some substantial advantages, such as longer stability, higher selectivity, lower limits of detection and high operating temperatures.

Depending on the used electrolyte, electrochemical sensors can be applied in real matrices at temperatures from −30 ˚C up to 1600 ˚C. The conventional electrochemical sensors using liquid electrolytes are usually limited to about 140ºC. In contrast, solid-electrolyte based sensors operate in the temperature above 500 ˚C. A case of solid electrolyte sensor is the yttria-stabilized zirconia based oxygen and hydrocarbon sensors [81].

The main types of electrochemical sensors are:

- Potentiometric sensors
- Conductometric sensors
- Amperometric sensors

At potentiometric sensors a local equilibrium is established at the sensor interface and either the electrode or membrane potential is measured. The potential difference between two electrodes converts into measurable information about the composition of the sample. Conductometric sensors measure the conductivity at a series of frequencies. As for amperometric sensors, a potential is applied between a reference and a working electrode,

causing the oxidation or reduction of an electroactive compound and afterwards measuring the resultant current. Amperometric sensors will be widely reviewed in the next chapter.

2.5.2 Potentiometric Sensors

Potentiometric devices measure the potential at the working electrode compared to the reference electrode in an electrochemical cell (Fig. 2.6), when ideally zero or no significant current flows between them [82]. The relationship between the concentration of the compound of interest and the potential is controlled by the Nernst equation. Potentiometry provides information about the activity of ions in an electrochemical reaction [83].

The lowest detection limits for potentiometric devices are achieved with ion-selective electrodes. Potentiometric sensors are suitable for measuring relatively low concentrations in minute volumes, since they do not react and chemically influencing a sample. Response time mainly depend on the rate of the establishment of the equilibrium at the sensor interface.

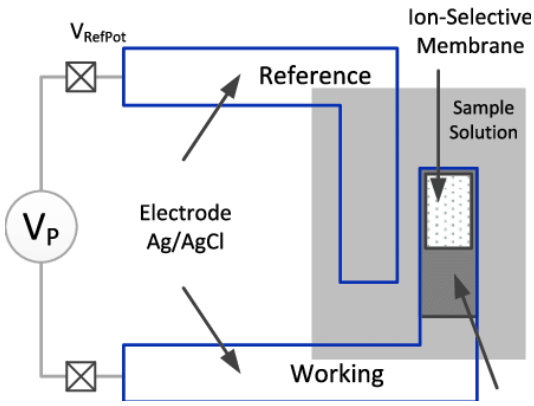

Figure 2.6. A typical potentiometric sensor scheme [84].

The three basic types of potentiometric devices consist ion selective electrodes, coated wire electrodes and field effect transistors electrodes, which work as an extension of the coated wire electrodes. Particularly, ion selective electrode is an indicator electrode, with the ability of selectively measuring the activity of a particular ion.

The pH electrode is one the most extensively used potentiometric devices, due to its simplicity, rapidity, low cost, while being applicable to a wide concentration range and exceptional selective for hydrogen ions. Nevertheless, measurements of pH can be also

accomplished using other types of potentiometric sensors. Glass electrodes based on thin ion-sensitive glass membrane are also widely exerted, in many different sizes and shapes, for the detection of substances, such as sodium, lithium [85], ammonium and potassium [86].

2.5.3 Conductometric Sensors

Conductometric sensors are the simplest of the electroanalytical applications, but fundamentally non-specific and non-selective. The concentration of the charge is obtained through the measurement of solution resistance, typically measured from a DC current, although the measurement can also be done with an AC current.

Conductometric sensors can observe the changes of electric conductivity of a film or a bulk material, whose conductivity is affected by the present analyte. Conductometric methods provide convenient properties, such as simplicity, as there is no need for reference electrode and low cost. Modified electrodes have contributed to the improvement of this technique, by making the measurement of the conductivity more rapid and accurate, thus enhancing the determination of analytes in the sample.

Thin films are used mostly as gas sensors, due to their conductivity changes following surface absorption. CdS films can be utilized as oxygen sensors, due to oxygen absorption [87]. Porous films of MnWO4 can work as a humidity [88]. The detection of H_2S can be achieved, as oxides doped with copper or copper oxide are very sensitive to gases containing this substance [89], while CH_4 can be detected by semiconducting Ga_2O_3 thin films [90]. Polymers are also exploited; Volatile amines and NH_3 can be detected with the use of polypyrrole [91].

The current development in sensor technology is focused on manufacturing of sensors with immediate response for the determination of components in the milliseconds-time scale, application of multisensor setups for measuring different ions concentrations and pH, minimizing sensors size for measurement inside biological systems, organisms and cells, expand of solid-state sensors to low temperatures and development of upgraded sensor materials, to enhance the selectivity, sensitivity, and stability.

CHAPTER 3: Electrochemical amperometric sensors

3.1 Basic theory

The amperometric sensor produces current signal, with the application of a certain potential between the working and the reference electrode [92]. The applied potential is the driving force for the transfer of electrons. The current that results is a direct measure of the rate of the electron transfer reaction, proportional to the concentration of the analyte, obeying Faraday's law. The measurement of a current at a constant potential is referred to as amperometry, while the measurement of a current during controlled variations of the potential current, this is referred to as voltammetry. The peak value of the measured current is directly proportional to the bulk concentration of the analyte [93].

The main operation of amperometric or voltammetric devices is the transfer of electrons to or from the analyte. For this purpose, potential-control equipment is required. The basic electrochemical cell consists of two electrodes in an applicable electrolyte. However, the typical set up is the three-electrode cell. The working electrode is the electrode at which the reaction of interest occurs. The reference electrode, which is most commonly Ag/AgCl, provides a stable potential compared to the working electrode. As for the auxiliary electrode an inert conducting material is usually used, like Pt. In order to eliminate electromigration effects and decline of solution resistance a suitable electrolyte must be employed. What is also noteworthy is that amperometric devices have greater sensitivity compared to potentiometric devices [94].

The working electrode heavily influences the performance of amperometric sensors, therefore much effort has been devoted to electrode fabrication and maintenance. The first electrochemical measurements of analytes started in 1922, when Heyrovsky invented the dropping mercury electrode, earning him a Nobel prize.

In the past the most suitable electrode materials for many years was mercury, as it has a prolonged potential range window and can easily be reproduced. The mercury film electrode was the most popular working electrode for stripping analysis. However, the limited anodic potential and toxicity are the fundamental drawbacks of mercury.

Following mercury electrode, the oxygen Clark electrode was introduced, which was used for monitoring the level of oxygen in water. Since, there have been many improvements; a prime example of an amperometric device is the glucose sensor (Fig. 3.1), based on the amperometric detection of hydrogen peroxide. Solid electrodes, such as carbon, platinum, nickel, copper, silver and gold have been the most popular as electrode materials, due to their versatile potential window, low background current and chemical inertness [95].

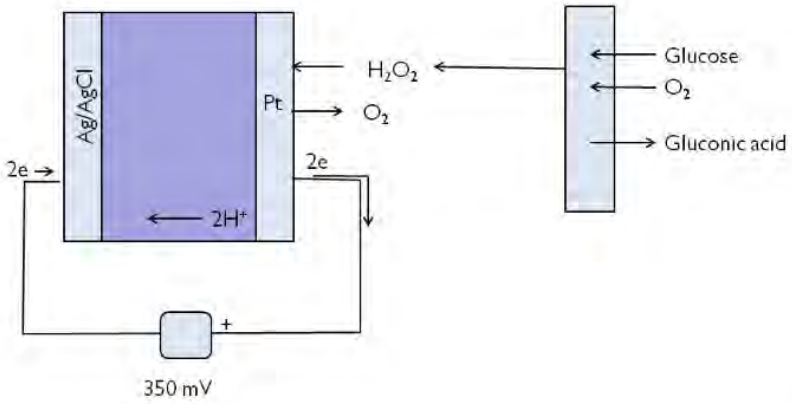

Figure 3.1. Basic setup of an amperometric glucose sensor [96].

Chemically modified electrodes are a recent development to electrode systems. The electrode surface alteration is conducted in each case with a suitable surface modifier. The miniaturization of the working electrode has also been examined, ensuing to the fabrication of microelectrodes with dimensions close to 2 mm or less. This can result to possible in vivo measurements. The outcome of this advance is the development of biosensors, capable of permitting a bio-specific reagent, retained or immobilized at the electrode, to convert a biological recognition process into a quantitative amperometric response. Despite their progress, until 1970's, amperometric sensors could not be applied to industrial fields and

could only be used only to strict laboratory conditions. The development of screen-printed electrodes has provided sensors that are potentially portable.

3.1.1 Chemically modified electrodes

Immobilization of chemical microstructures on electrode surfaces has been a major growth area in electrochemistry. Chemically modified electrodes result from an immobilization of a modifier agent on the electrode surface though chemical reactions, chemisorption, polymer coating or composite formation. Superior control of electrode characteristics and reactivity is achieved by this surface modification, compared to bare electrodes, since the immobilization transfers the physicochemical properties of the modifier to the electrode surface.

The strategy of coating an ion-exchange polymer on the electrode surface using solid electrodes modified with a layer of a polymer with properties promote the exchange of ions, which allows the detection of an analyte that can be oxidized or reduced. The signal produced depends on the concentration of the electroactive compound at the polymeric layer [97]. Furthermore, mili-molar concentration levels of analytes, which are electroactive can be detected, with the proper selection of an ion exchanger with good selectivity [98]. Although polystyrene sulphonate, polyvinyl sulphate, deprotonated polyacrylic acid and poly-L-lysine, Tosflex, polyvinylpyridine and cellulose acetate have received significant attention, the most popular cation exchanging system is Nafion [99].

A common approach for incorporating the modifier on the electrode is the cover of the surface with an appropriate polymer film. Most polymers are applied to electrode surfaces by the adsorptive attraction and low solubility in the electrolyte solution. Different types of inorganic films, such as metal oxide, clay, zeolite, and metal ferrocyanide, can also be formed on electrode surfaces. These films are beneficial, due to their well-defined structures, thermal and chemical stability, and relatively low cost [100].

Examples of potential application of such systems are the development of systems with good electrocatalytic activity, high chemical selectivity, electrodes with anticorrosive properties and electrochemical devices in tiny size for the field of molecular electronics and

electrochemical sensors. The main benefits of chemically modified electrodes to amperometric devices include higher selectivity, stability and detectability, by reducing the reaction time of these reactions involving transfer of electrodes, accumulation in preferential way, selectivity on the permeation on the membrane and exclusion of interferences [101].

3.1.2 Microelectrodes

Amperometric sensors ought to have small dimensions. This necessity led to the research of microelectrode systems. The miniaturization of the working electrode was first proposed by Wightman for the in vivo and in vitro detection of neurotransmitters [102]. Microelectrodes exhibit several capabilities, including the detection in microflow system, the exploration of microscopic domains, the in vivo monitoring of neurochemical events and analyses of very small sample volumes [103].

Electrodes of different materials have been miniaturized in many geometrical shapes. However, they have a common characteristic, as the diffusion layer at the surface is bigger than the electrode dimension. The signal response of microelectrodes is much better than the one of the conventional electrodes, due to the greatly reduced double-layer capacitance, which is associated with the small electrode area and radial diffusion to the edges. They can also operate in high resistive situations, such as solutions without proper electrolytic properties, low electricity and temperatures, due to various geometries and low current intensities. Carbon fibers, thin metal films, gold, platinum and iridium wires, are commonly used for these preparations.

3.1.3 Screen printed electrodes.

The demand for portable electroanalytical sensors, to execute clinical, environmental or industrial functions as well as applications in laboratory conditions, can be fulfilled with the screen printed electrode technology.

Screen printing is a simple, inexpensive and reproducible process for electrode deposition, usually using ceramic materials or PVC. The electrode can be coated with a conducting ink,

which is supported with an additional film with isolating properties. The purpose of the coating is to establish an electrical contact to the electrode surface. They can be portable, are relatively simple to operate, reliable and have a low manufacturing cost. The most successful have included noble metals and carbon. Carbon has a relatively low market price, conductive properties, attributes that make it the most used substrate for fabrication of low-cost electrodes. Chemically modified electrodes can also be produced by absorbing specific reagents to the screen-printed catalytic ink, which increases their selective and detective characteristics.

Amperometric sensors based on screen printed electrodes can determine biomolecular drugs, environmental toxins and industrial pollutants with great success. This technology is widely accepted in electrochemistry as these disposable sensors provide fast and simple detections. Many devices based on screen-printing are commercially available, such as the screen printed electrochemical sensors for blood glucose determination [104].

3.2 Electrochemical thermodynamics and kinetics

3.2.1 Faraday's Law

Faraday's laws of electrolysis are quantitative relationships based on the electrochemical researches published by Michael Faraday in 1834. In electrochemistry, Faraday's law can be used to find the amount of substance deposited at an electrode, the number of electrons implicated in an electrolytic process and the total amount of electricity required for complete the electrolysis of a compound can be also found by the Faraday's law.

Faraday cased two laws of electrolysis. The first states that the mass of a substance altered at an electrode during electrolysis is directly proportional to the quantity of electricity transferred at that electrode. It should be noted that the quantity of electricity refers to electrical charge, typically measured in coulombs, and not to electrical current. Faraday's second law cites that for a given quantity of electricity, the mass of an elemental material altered at an electrode is directly proportional to the element's equivalent weight. The

equivalent weight of a substance is its molar mass divided by an integer that depends on the reaction undergone by the material.

The mathematical form of Faraday's laws can be represented by:

$$m = \frac{Q}{F} \cdot \frac{M}{Z} \tag{3.2}$$

where m is the mass of the substance altered at an electrode, Q is the total electric charge passed through the substance, F = 96.485 C mol^{-1} is the Faraday constant, M is the molar mass of the substance, and z is the number of ions of the substance, electrons transferred per ion.

Note that M/z is the same as the equivalent weight of the substance altered. For Faraday's first law, M, F, and z are constants, so the larger the value of Q, the larger will M be. For Faraday's second law, Q, F, and z are constants, so the larger the value of M/z, the larger will M be [105].

Another useful form of Faraday's law, which relates the total charge Q that passes through an electrochemical cell to the amount of product N is:

$$Q = n \cdot F \cdot N \tag{3.2}$$

where F is Faraday's constant and n is the number of electrons transferred per mole of product.

3.2.2 Limiting Current

While increasing the applied potential during a redox reaction, an abrupt rise of the current is observed until it reaches a maximum, indicating that the current value is stabilized regardless of any further applied voltage. The current may rise again, but only when the potential receives significant greater values. This current "plateau" indicates that a particular electrode reaction proceeds at the highest possible rate (Fig. 3.2). Limiting current describes the maximum rate at 100% current efficiency, at which this reaction can proceed in the steady state.

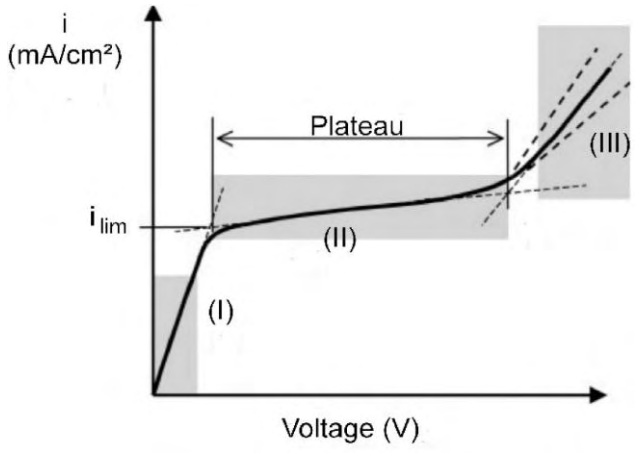

Figure 3.2. Current-voltage curve to determinate the limiting current density by transition between regions I and II [106].

The existence of the limiting current indicates the slowness of transport of charged or uncharged molecules and ions respectively through the solution. We can say that these species are consumed in the electrode reaction. Limiting current density is observed when the supply of a transferred species to the electrode surface is a rate-limiting factor [107].

3.2.3 Nernst Equation

The movement of electric charge through a conductor depends on and the potential difference and the amount of the charge that is moved. The potential difference is the difference in electric potential between two points and is measured in volts. At an electrochemical cell, the potential difference voltage between the electrodes is less than the maximum possible voltage of the cell.

This deficit of the voltage occurs due to the energy that is required for the process and the flow of the electric current. It only reaches its maximum value only when no current flows. The maximum voltage of a cell is referred to as Electromotive Force and it depends on the temperature, concentration and pressure of the cell. Given that the measurement takes place under standard states, which are temperature 25°C, concentration 1M, pressure 1 atm, the cell voltage is referred to as standard state cell potential E^{o}_{cell}. The sum of the half-cell potential of the reduction and the oxidation is called cell potential.

$$E_{cell} = E_{reduction} + E_{oxidation} \quad (3.3)$$

or

$$E_{cell} = E_{cathode} + E_{anode} \quad (3.4)$$

Walther Hermann Nernst was a German chemist who is known for his work in thermodynamics. The formulation of the Nernst heat theorem paved the way for the third law of thermodynamics, winning him the Nobel Prize in Chemistry, in 1920. Nernst helped establish the modern field of physical chemistry and contributed to electrochemistry, thermodynamics and solid state physics. He is also known for developing the Nernst equation in 1887.

The Nernst Equation is the fundamental principle, which relates electromotive force, or potential, to thermodynamic properties. It can be used to find the cell potential at any moment during a reaction or at conditions other than standard-state. Redox reactions can generally be expressed in the following format where an oxidant, Ox, results to a reductant product, Red, by the charge transfer of n number of electrodes:

$$Ox + ne^- \Leftrightarrow Red \quad (3.5)$$

This electrochemical redox reaction occurs at a potential, set as E, which is related to the standard potential of the reaction, set as E^o_{cell} and the concentrations of the reactants and products by:

$$E = E^0_{cell} + \frac{RT}{nF} \ln \frac{C_{ox}}{C_{red}} \quad (3.6)$$

where R is the gas constant, T is the temperature in Kelvin, n is the number of electrons transferred at the redox reaction, F is Faraday's constant, and C_{ox}, C_{Red} represent the concentration of the oxidation and reduction species at the electrode interface. For this common expression of the Nernst equation, the activity coefficients of Ox and Red are assumed to be at unity.

The basic thermodynamics for a reversible electrochemical reaction is given by:

$$\Delta G = \Delta H - T\Delta S \quad (3.7)$$

where ΔG is the Gibbs free energy or the available energy in a reaction, ΔH is the enthalpy, or the energy released by the reaction, ΔS is the entropy and T is the absolute temperature, with TΔS being the heat associated with the reaction. The terms ΔG, ΔH and ΔS are state functions and depend only by the characteristics of the electrode materials and the initial and final states of the reactions [108]. The Nernst Equation relates the potential of an electrochemical reaction to some fundamental thermodynamic properties, as described in the following equation:

$$\Delta G^{o} = -nFE^{o}_{cell} \tag{3.8}$$

where ΔG° is Gibbs free energy, n represents number of electrons transferred at the redox reaction, F is Faraday's constant, and $E°_{cell}$ is the abovementioned potential at standard conditions. The Nernst equation applies to a redox reaction at steady state conditions[109].

Overpotential is the potential difference between a half-reaction's thermodynamically determined reduction potential and the potential at which the redox event is experimentally observed. The term is directly related to a cell's voltage efficiency. Typically, in an electrolytic cell the overpotential requires more energy than thermodynamically expected to drive a reaction. On the other hand, in a galvanic cell, overpotential means that less energy is recovered than the energy that can be predicted by thermodynamics. Non negligible is also the fact that it describes the potential losses required to drive an electrochemical reaction. Since the Nernst equation is linked to thermodynamic properties, the overpotential describes the thermodynamic efficiency of a redox reaction.

Overpotential is a quantity specific to each cell design and varies across cells and operational conditions. In a nutshell, the overpotential, η:

$$\eta = E^{0}_{cell} - E \tag{3.9}$$

is the difference between the theoretical, E^0 and operating potential, E.

3.2.4 Butler-Volmer Equation

John Alfred Valentine Butler was an English physical chemist best known for his contributions to the development of electrode kinetics. He was awarded the Meldola Medal and Prize in 1928 by the Royal Institute of Chemistry. Max Volmer was a German physical

chemist, who also made important contributions on electrode kinetics and on electrochemistry in general. Both co-developed the Butler–Volmer equation.

The Butler-Volmer Equation is a kinetic relationship between current and overpotential of an electrochemical device. The terms in the equation each have their own importance and are linked to fundamental scientific principles and will be discussed independently. Both Butler and Volmer are credited with the development of the relationship and published their findings simultaneously. The Butler-Volmer Equation is expressed as:

$$I = I_0 \left(\exp \frac{anF}{RT} n \; - \; \frac{(1-a)nF}{RT} n\right) \tag{3.10}$$

where R is the gas constant, T is the temperature, I is the current and I_0 is the exchange current of the electrochemical cell, α is the transfer coefficient, n is the number of electrons transferred, F is the Faraday Constant and n is the overpotential.

The exchange current density is a pre-exponential term in the Butler-Volmer equation and describes the current that the electrochemical cell is theoretical capable of producing without activation influences or other losses. The exchange current density is described at open circuit potential, where there is no net current and the forward and reverse reactions are occurring at the same rate which is equal and opposite in magnitude. The forward and reverse components can be considered idle and upon polarization, will produce a net current. High exchange current density means that the redox reaction occurs rapidly in both directions

The way the current will be kinetically affected by polarization, is indicated by the other parameters in the exponential expression. The Faraday constant, gas constant, current and temperature maintain their typical meaning in this equation. The transfer coefficient is a dimensionless parameter that relates the properties of the transition state for the forward and reverse reactions of the reacting species in the electrochemical system [110].

3.2.5 Tafel Equation

The Tafel equation was empirically developed by Julius Tafel in 1905 and later named Tafel equation in his honor. Tafel experimentally measured the hydrogen evolution

reaction on several metal electrodes such as mercury, lead, and cadmium. He researched the relationship of overpotential, rather than the absolute potential and the logarithm of current density and was aiming to control the rate of electrode reactions by controlling potential. At the time of discovery, it is presumed that Tafel did not fully realize the contribution he made to the field of electrochemistry and not speculate the meanings of the physical constants of the equation he reported:

$$\eta = a + b \log(J) \tag{3.11}$$

where η is the overpotential, a is the intercept of the Tafel plot, b is the slope of the fitted line on a Tafel plot and J is the scalar current density. Since Tafel's reports in 1905, it has been shown that his empirical relationship can be related to fundamental principles. The establishment of the Butler-Volmer equation occurred about 27 years after Tafel published his work, confirming that the Tafel equation stems from fundamental electrochemical principles, as the Tafel Equation can be derived from the Butler-Volmer equation, which is a relationship of fundamental terms.

In the Tafel region, the electrode polarization is sufficient enough to suppress the reverse reaction and the forward reaction dominates. Thus, the reverse reaction branch in the Butler-Volmer equation is negligible and the equation is reduced to:

$$I = I_0 \exp \frac{anF}{RT} n \tag{3.12}$$

Rearrangement of the terms, with the addition of the quantity 2.303 accounts for the differences in the natural logarithm used in the Butler-Volmer equation and the base 10 logarithm used in the Tafel equation:

$$\log(I) - \log(I_0) = \frac{anF}{2.303rT} n \tag{3.13}$$

Solving for η yields to:

$$n = \frac{2.303rT}{anF}\log(I) - \frac{2.303rT}{anF}\log(I_0) \tag{3.14}$$

which resembles the form of a line where b is the slope and a is the intercept, where the slope of the line on a Tafel plot is represented by:

$$b = \frac{2.303rT}{anF} \tag{3.15}$$

and the intercept of the line is an expression of these constants

$$a = -\frac{2.303rT}{anF}\log(I_0) \tag{3.16}$$

This derivation of the Tafel equation shows its relationship to kinetic properties. Kinetics Thermodynamics describe reactions at equilibrium and the maximum energy available for a given reaction [111].

Separating the parameter a_a to ascorbic acid and a_c, which are called anodic and cathodic transfer coefficients respectively we can relate how an applied potential favors one direction of reaction over the other [112]. The following equations can be extracted:

$$\text{Oxidation slope} = -\frac{a_a nF}{2.303rT}n \tag{3.17}$$

$$\text{Reduction slope} = -\frac{a_C nF}{2.303rT}n \tag{3.18}$$

Corrosion rates can be measured by Tafel extrapolation and polarization resistance. For an electrochemical reaction under activation control, polarization curves exhibit linear behavior in the E(V) vs Log Absolute Current(A) Tafel plots (Fig. 3.3). That is referred to as Tafel behavior.

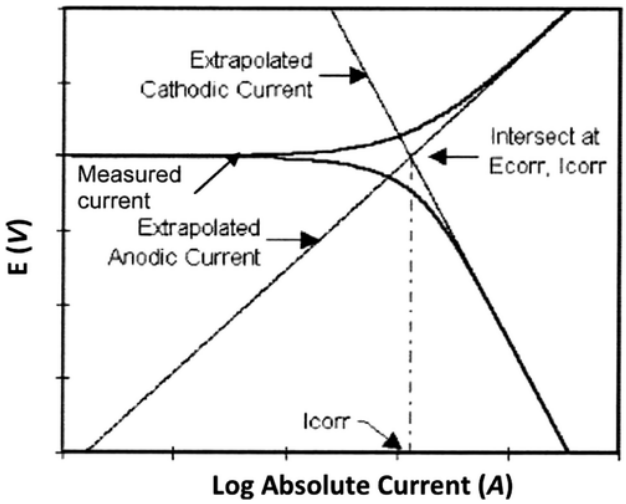

Figure 3.3. Schematic polarization curve showing Tafel extrapolation [113].

At the E_{corr} corrosion potential, the rate of cathodic reduction is equal to rate of anodic reaction, where metal corrosion occurs. The slope of the linear region on the Tafel plot can be used to calculate the transfer coefficient a. However, they are not independent variables and in most of the cases: ascorbic acid + $a_c = 1$.

3.2.6 Koutecky-Levich Equation

The Koutecky-Levich equation is a versatile tool that is commonly used for the correction of mass transport effects in a rotating disc electrode testing to obtain kinetic current densities. The Koutecky-Levich equation can be derived from two basic assumptions. The first is a linear diffusion model of reactants, where the surface reactant concentration C_a can be related to the reactant concentration in the bulk C_b by the measured total current density I_m and the mass transport limiting current density I_{lim}.

$$\frac{C_a}{C_b} = \frac{I_{lim} - I_m}{I_{lim}} \tag{3.19}$$

The second assumption is that the electrochemical reaction follows first-order reaction kinetics. Assuming a first order reaction, the local current density I_{loc} is proportional to the multiplication of surface reactant concentration and the kinetic current density I_k, whereby I_k

is a function of overpotential n and is a product of reaction rate constant and reactant concentration C_a under standard conditions:

$$I_{loc} = I_k \frac{C_a}{C_b} \tag{3.20}$$

As $I_{tot} = L\ I_{loc}$ and given that the surface roughness factor L of the electrode is 1, the previous equations can be combined to form the Koutecky-Levich equation [114]:

$$\frac{1}{I_m} = \frac{1}{I_{lim}} + \frac{1}{I_k} \tag{3.21}$$

In the case of the rotating disk electrode, the equation is deduced to:

$$\frac{1}{I_m} = \frac{1}{BL\omega^{0.5}} + \frac{1}{I_k} \tag{3.22}$$

where BL is the Levich constant and ω is the angular rotation rate of the electrode.

Inverse measured current is plotted versus the inverse square root of rotation rate to obtain the Koutecky-Levich plot (Fig. 3.4), with a slope of BL^{-1}.

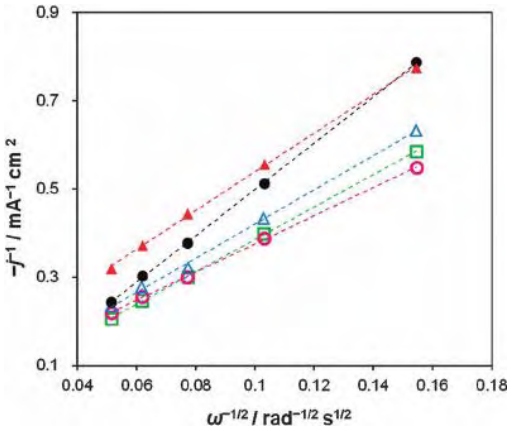

Figure 3.4. Experimental Koutecky-Levich plot using rotating disc electrode [115].

CHAPTER 4: Experimental Part

4.1 Experimental techniques

The experimental techniques used to determinate the structure and electrochemical behavior of Pt (20%wt)/graphitized carbon and Pd (20%wt)/Vulcan-XC72 electro-catalyst is described in this chapter. Specifically, in order to characterize the structure and the composition of the catalysts, the physicochemical technique employed was transmission electron microscopy (TEM). Moreover, many different electrochemical techniques were used, such as cyclic voltammetry (CV), rotating disk electrode (RDE) and chronoamperometry (CA), in order to evaluate the catalytic activity and investigate whether is suitable for the detection of ascorbic and uric acid.

4.1.1 Transmission electron microscopy

Max Knoll and Ernst Ruska were the first to build a transmission electron microscope in 1931 and widely used later in 1936 with great success. Transmission electron microscopy is a microscopy technique that uses beam of energetic electrons generated by thermionic emission from a filament. Afterwards, an image is created, due to the electrons interaction with the ultra-thin sample, as it passes through. A transmission electron microscope consists of many parts, such as an electron emission source for generating of the electron stream, a vacuum system, in which the electrons travel, electrostatic plates and a series of electromagnetic lenses. Also, a device is required in order to allow the insertion into, motion within, and removal of specimens from the beam path. Subsequently, imaging devices are used to create an image from the electrons that exit the system. TEMs are capable of imaging at a significantly high resolution, due to the small de Broglie wavelength of electrons. This allows for examination of single columns of atoms which are in the region of nanometers, hence it has found application in nanoscience and nanotechnology research [116].

4.1.2 Cyclic Voltammetry

The cyclic voltammetry linear scanning technique is the most commonly used and generally known technique for the study of electrochemical reactions. Cyclic voltammetry is based on cycling the potential of an electrode, which is immersed in an unstirred solution. The resulting current is measured versus a reference electrode such, as a saturated calomel electrode, or a silver-silver chloride (Ag/AgCl) electrode. The controlling potential applied across these two electrodes is the excitation analytical signal.

The signal of a cyclic voltammetry is a linear potential scan with a triangular waveform (Fig. 4.1). This triangular potential signal sweeps the potential of the electrode between two values, which are called the switching potentials. In the figure below, the section 1-2-1' is the first cycle and the section 1'-2'-1'' is the second cycle of the scanning. In particular, the ascending parts 1-2 and 1'-2' represent the anodic scanning, while the descending parts 2-1' and 2'-1'' represent the cathodic scanning. During anodic oxidative reactions are carried out, while reductive reaction can be observed reactions at cathodic scans.

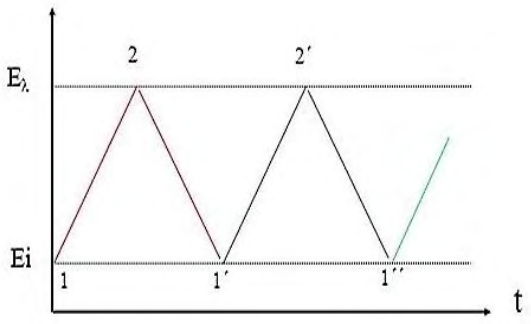

Figure 4.1. Triangular shift of the potential at a cyclic voltammetry experiment [117].

The velocity of the scanning, which is referred to as scan rate, is reflected by the slope, which is the derivative of:

$$V = \frac{dE}{dt} \text{ (V s}^{-1}\text{)} \tag{4.3}$$

As the scan rate remains constant, the current passing through the surface of the electrode is a function of the velocity and time. Depending on the capabilities of the potentiostat, the velocity of a scanning ranges from a few mV s^{-1} to 10^6 V s^{-1}. The shape of a cyclic

voltammogram is influenced by the scan rate, the speed of the mass transfer at the surface of the electrode and the load transfer during the main reaction. In reversible electrochemical reactions the load transfer speed is much greater than the diffusion rate, so the kinetics are substantially controlled by the diffusion.

A cyclic voltammogram is obtained by measuring the current at the working electrode during the potential scan, resulting to current-potential curves. The current can be considered the response signal to the potential signal. The voltammogram is a display of current, depicted at the vertical axis versus potential, illustrated at horizontal axis [117].

4.1.3 Chronoamperometry

Chronoamperometry requires the potential of the working electrode to be stepped from a value, at which no Faradaic reaction occurs, up to a potential of zero surface concentration. In chronoamperometry the current is measured as a function of time. As demonstrated at Fig. 4.2, when the potential is at E_1, no current flow and no oxidation or reduction of the electrochemically active species takes place. In contrast, when the potential reaches E_2, the current flows and the electrochemical reaction occurs, which is diffusion limited.

The current in chronoamperometry is a function of time. The application of the potential step obeys the Cottrell equation, which describes the observed current at any time in a reversible redox reaction:

$$I(t) = \frac{n\ F\ A\ c\ D^{1/2}}{\pi^{1/2} t^{1/2}} = k\ t^{-1/2} \tag{4.2}$$

Where n is stoichiometric number of electrons involved in the reaction, F is the Faraday constant, A is the surface area, c is the concentration of the electroactive species, D is the diffusion coefficient and t represents time.

Chronoamperometry experiments are either single potential step, as described above, or double potential step, in which the potential is returned to a final value E_f following a time period τ.

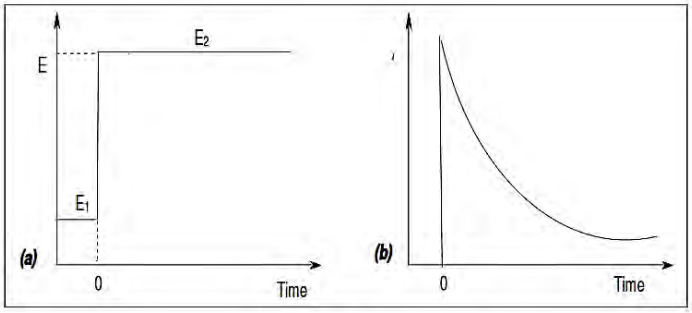

Figure 4.2. Current-time curve of a chronoamperometry [118].

The potential step sequence is shown at Fig. 4.2. A forward potential step from the Ei to Es occurs at a τ duration. The reverse potential step ends up to the final potential Ef, which generally equals the initial Ei. The current on the reverse step is also recorded for a time equal to τ [118].

4.1.4 Rotating disk electrode

The Rotating electrode technology, which includes rotating disk electrode and rotating ring-disk electrode techniques, is one of the important electrochemical measurement methods. Using a rotating disc electrode assists the mechanisms and kinetics of the reaction of interest on the electrode. Rotating disk electrode and rotating ring-disk electrode exhibit substantial advantages in measuring reaction kinetic constant, reaction electron transfer number, reactant concentration and diffusion coefficient. The collected data can be processed with the assistance of the Koutecky-Levich theory.

In order to have an adequate mass transport of the reactants with high reproducibility, the use of the rotating disk electrode technique is one of the elite methods. Although there are ways to increase the rate of mass transfer, most commonly with stirring, it is more efficient to rotate the electrode inside the analyte solution rather than using a magnetic stirrer. Rotating disc electrode is consisted by a cylindrical metal rod embedded into the bottom face of an insulating cylindrical plastic holder. Teflon is a prime example of insulating material. The electrode is cut and polished together with the holder so that only the bottom

edge of the metal cylinder can contact with the solution. The rotating disk electrode technique is used for solid electrodes.

The most important property of the rotating disc electrode is that the rate of mass transport at the electrode surface is even and homogeneous, due to the linear velocity of each unique point on the surface, increased proportionally by its distance from the center axis of rotation (Fig. 4.3). Another significant aspect of the rotating disc electrode is the laminar flow around the electrode, even if it is rotated at high speed.

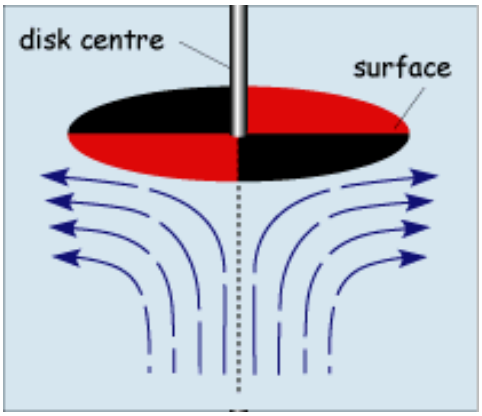

Figure 4.3. Rotating disk electrode solution velocity profile [117].

The transition from laminar to turbulent flow depends on Reynolds number, a non-dimensional variable. The equation for Reynolds number is:

$$\mathrm{Re} = \upsilon \frac{l}{\nu} \tag{4.3}$$

where Re is obviously Reynolds number, υ is the characteristic velocity, l is the characteristic length and ν is the kinematic viscosity, the ratio of the dynamic viscosity μ to the density of the fluid ρ. The characteristic velocity of a rotating disc electrode is the linear velocity at outer edge of the disc electrode, so Reynolds number is:

$$\mathrm{Re} = \omega r \frac{r}{\nu} = \omega \frac{r^2}{\nu} \tag{4.4}$$

Which results in $\mathrm{Re} < \mathrm{Re}_{crit}$, where $\mathrm{Re}_{crit} = 10^5$ is the critical Reynolds number, for a typical electrode of 0.3 cm radius of 0.3 cm, under a variety of angular velocities and rotations per minute.

The electrode surface is a crucial factor that affects the critical Reynolds number. If the surface is smooth, without manufacturing flaws, the critical number Reynolds represents the upper limit for a laminar flow, in contrast with a rough surface, where turbulent flow can be witnessed, even with inferior Reynolds number [117].

4.2 Experimental Procedure

The electrochemical experiments took place in a potentiostat AMEL 7050 (Fig.4.4.A), in an electrochemical cell of three electrodes (Fig.4.4.B). Platinum tip and Ag/AgCl (0.1 mol L^{-1} KOH) were used as counter and reference electrodes respectively (Fig.4.5.A, B).

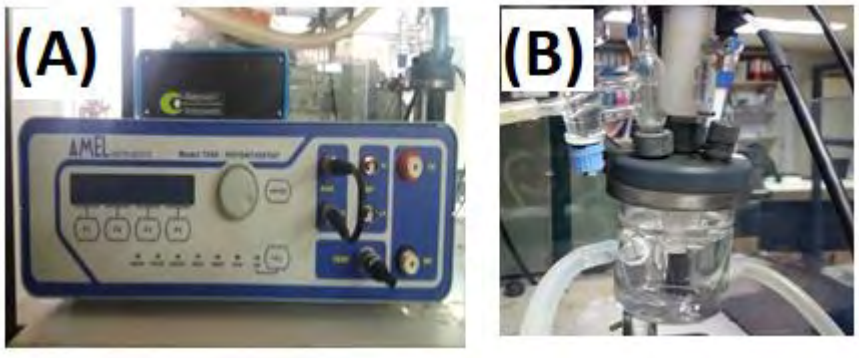

Figure 4.4. A) AMEL 7050 Potentiostat, B) Electrochemical cell

A glassy carbon disk electrode with diameter of 0.5 cm is used as the working electrode. This working electrode was coated with two different catalysts, Pt(20%wt)/graphitized carbon and Pd(20%wt)/Vulcan-XC72. The catalytic ink was composed by 5mg of the selected catalyst powder, 1.8ml Ethanol and 0.2ml Nafion. Nafion is consisted by a tetrafluoroethylene main chain with perfluoroether side chains and terminated with a sulfonic acid group, whose ionization yields an anionic Nafion membrane.

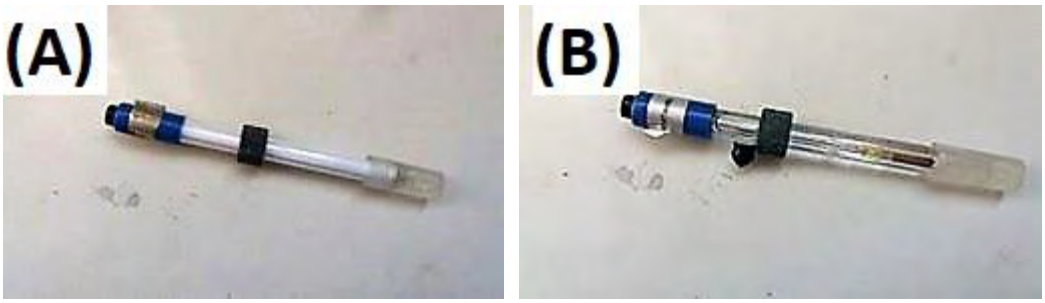

Figure 4.5. A) Counter electrode, B) Reference electrode

Ethanol and Nafion were added gradually to the mixture. First, the catalytic powder was mixed with Ethanol and afterwards, the mixture was homogenized in the magnetic stirrer (Fig.4.6.A) for 2 minutes and in the ultrasonicator for another 2 minutes (Fig. 4.6.B). This procedure was repeated for 3 times. Then, Nafion was added and the mixture was placed at the magnetic stirrer for 45 minutes. The mixed paste was then inserted into a glass tube (d: 1.5 mm). Before use, the surface of the glassy carbon electrode was smoothed using a mixture of alumina and deionized water and placed in the ultrasonicator for 10 minutes.

Figure 4.6. A) Magnetic stirrer B) Ultrasonicator

After the electrode was cleaned and dried, 10 μl of the mixed paste was placed on it. The modified electrode obtained was inserted in the solution and connected to the electrochemical station ready to use. Every time before the experiments, the solution was saturated with high-purity N_2 gas for 30 minutes in order to remove the dissolved oxygen in the electrolyte. The electrochemical techniques that assisted to the evaluation and comparison of the performance of the catalysts for ascorbic and uric acid were mainly the cyclic voltammetry and the chronoamperometry.

CHAPTER 5: Results and discussion

5.1 Pt(20%wt)/graphitized carbon electrocatalyst

In this chapter the results of the physicochemical and electrochemical characterization of the commercial Pt(20wt%)/graphitized carbon for ascorbic and uric acid electro-oxidation are reported. More precisely, the catalyst structure was characterized by transmission electron microscopy (TEM). The electrochemical characterization conducted via cyclic voltammetry (CV) and chronoamperometry (CA).

5.1.1 Physicochemical characterization

The surface morphology of the prepared Pt(20%wt)/graphitized carbon catalyst was examined by TEM. TEM images in Fig 5.1.a and Fig 5.1.b exhibit a successful loading dispersion of Pt/C nanoparticles onto the surface of carbon substrate.

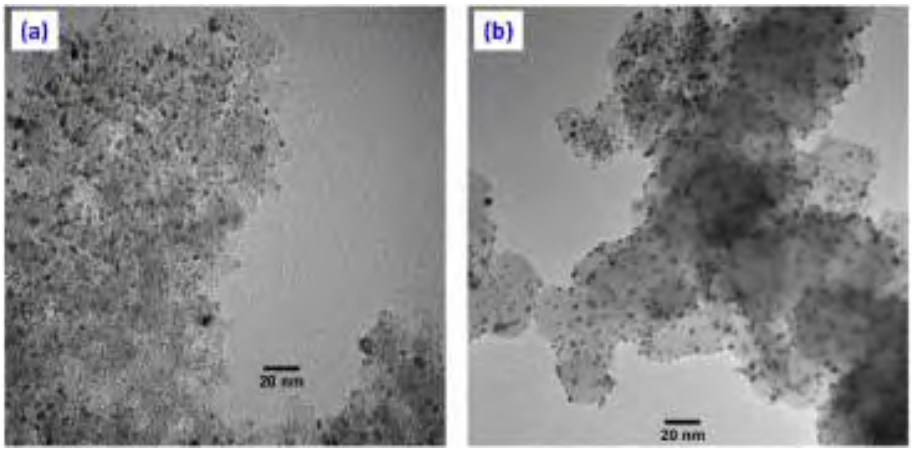

Figure 5.1. TEM images of Pt(20%wt)/graphitized carbon.

5.1.2 Electrochemical characterization

The electrocatalytic activity towards ascorbic and uric acid oxidation was examined by cyclic voltammetry. The stability and poisoning rate during time was investigated by chronoamperometry. The glassy carbon electrode (GCE) is modified using Pt(20%)/graphitized carbon for the electrochemical determination of low concentration, 0.5 mM of uric acid (UA) and 0.5 mM of ascorbic acid (AA) in pH 7.3 physiological buffer solution.

Cyclic voltammetry has been carried out initially, in 0.15 M physiological buffer solution **(**PBS) in absence and in presence of 0.5 mM uric acid in order to determine were the oxidation of uric acid takes place. As it is observed in Fig.5.2 (B), there are two curves that are noteworthy, one around 0.38-0.42 V and the other at 0.77-0.81 V. The first one is explained by hydrogen absorption and the second due to the uric acid oxidation.

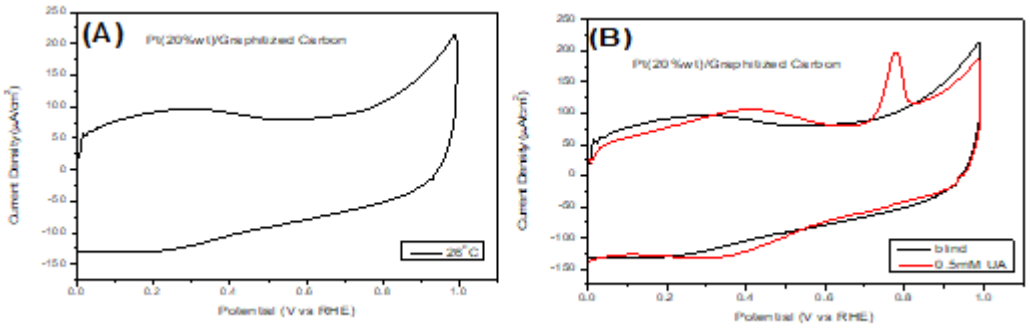

Figure 5.2. Cyclic voltammograms of the Pt(20%wt)/graphitized carbon in:(A) 0.15 M PBS, (B) 0.5 mM uric acid in a 0.15 M PBS (physiological buffer solution), (20 mV s^{-1}, 26 ^{o}C).

Over the past couple years, many scientists have tried to electrochemically detect uric acid using Pt based catalysts. Similar results can be found at a work where researchers have fabricated a hierarchical nanoporous PtCu alloy in order to electrochemically determine uric acid[41]. The sensor exhibits high electrochemical activity towards the oxidation of the compound at 0.61 V which is very close to this work and displays a wide linear response to UA in the range from 10 to 70 μM with the lower detection limit at 5.7μM.

Another work constructed a Pt/Au hybrid film electrode which showed efficient electro-catalytic functions towards the oxidation of uric acid. The oxidation took place at 0.54 V at

the bare electrode and as for Pt/Au hybrid film it occurred at 0.52 V. The potential shift and current increase shows the good catalytic activity of Pt/Au hybrid film modified electrode on the individual electro catalytic oxidation [33]. Last but not least, a graphene/Pt-modified glassy carbon (GC) electrode was fabricated to characterize uric acid levels via cyclic voltammetry and differential pulse voltammetry (DPV) by measuring the anodic peak potential at 0.4 V [119].

Table 5-1: Comparison of modified electrodes in the literature with this work.

Working Electrode	**Reference Electrode**	**Methods**	**Concentration Range (μM)**	**Peak Potential(V)**	**Detection Limit(μM)**	**Refs**
hnp-PtCu	RHE	CV, DPV	10.0-70	0.61	5.	[41]
Pt/GCE	Ag/AgCl	CV, DPV	21-336	0.52	21	[33]
gr/Pt/GCE	Ag/AgCl	CV, DPV	0.05-12	0.4	0.05	[119]
Pt/C/GCE	RHE	CV, CA	50	0.78	-	This work

The effect of temperature on uric acid's electro-oxidation was examined at four different temperature values, 26 ºC, 36 ºC, 46 ºC and 56 ºC. Fig. 5.3 shows the cyclic voltammetries for uric acid oxidation at different temperature values. In each cyclic voltammetry the open circuit is around 0.23 V and the scan rate is 20 mV s^{-1}.

The current density values are found to be 193.2 μA cm^{-2}, 266.37 μA cm^{-2}, 444.72 μA cm^{-2} and 583.79 μA cm^{-2} at 26 ºC, 36 ºC, 46 ºC and 56 ºC, respectively. With the rise of temperature, the peak is increased as well, demonstrating the increase of kinetic energy of the molecules and thus confirming the dependence of current from temperature.

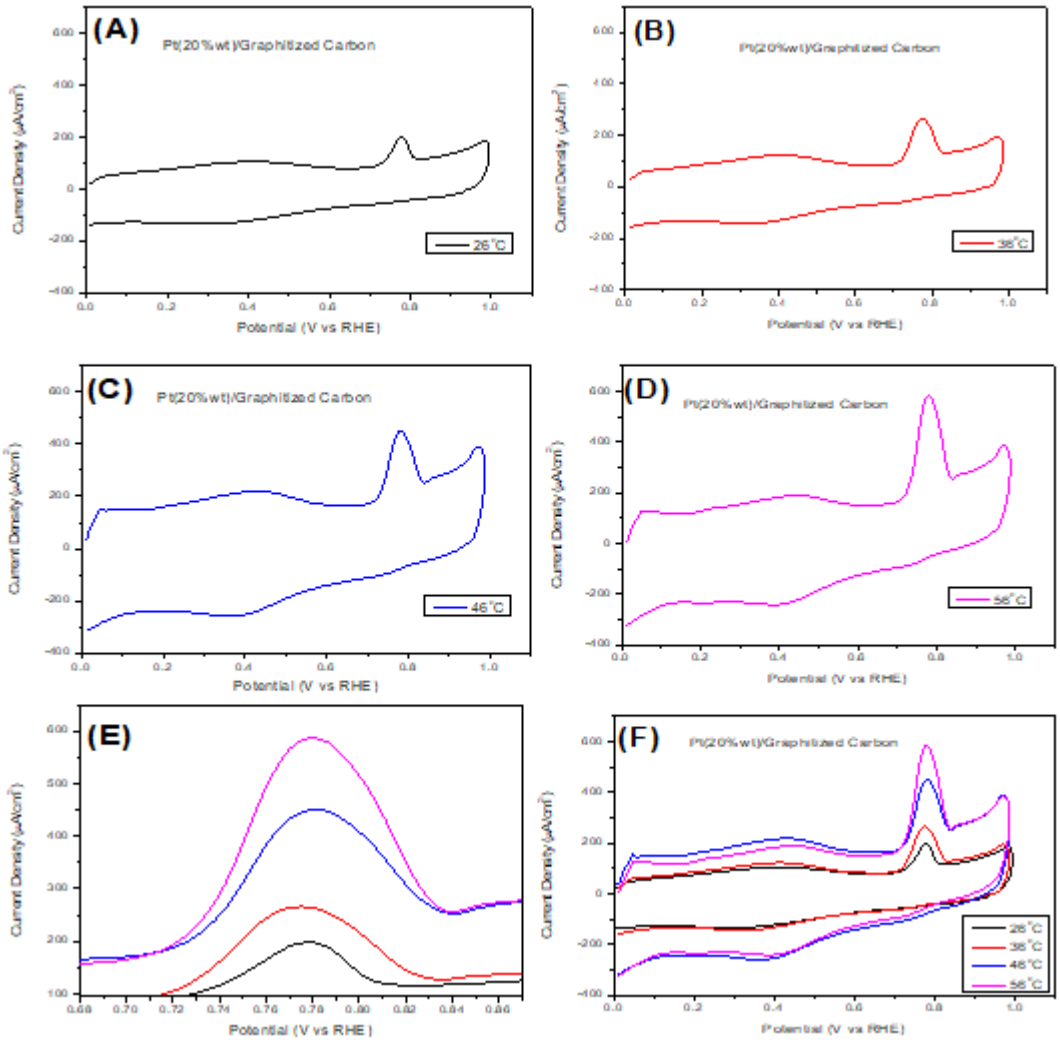

Figure 5.3. Cyclic voltammograms of Pt(20%wt)/graphitized carbon electrocatalyst in 0.5 mM uric acid in a 0.15 M PBS at: (A) 26 ºC, (B) 36 ºC, (C) 46 ºC, (D) 56 ºC, (20 mV s^{-1}), (E) Focus on oxidation peak current, (F): Comparison of all previous cyclic voltammograms.

Activation energy E_a is calculated from the following equation [120],

$$E_a = R\frac{d(\ln I)}{d(1/T)} \tag{5.4}$$

where R is the gas constant, I the current and T the absolute temperature (K). Taking into consideration Fig. 5.4.(Arrhenius plot), activation energy E_a was calculated to be 31.8 kJ mol^{-1} which is a satisfactory value according to the literature [121].

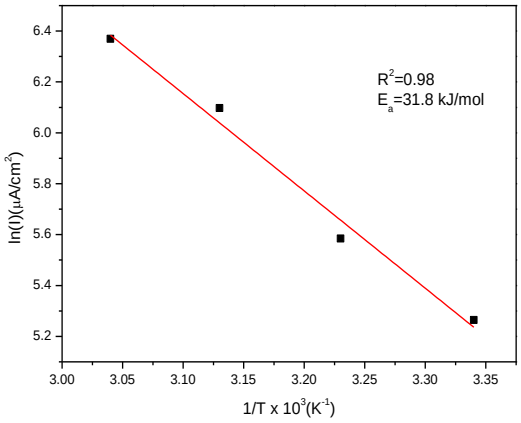

Figure 5.4. Arrhenius plot for the Pt(20%wt)/graphitized carbon electrocatalyst in 0.5 mM uric acid in a 0.15 M PBS derived from cyclic voltammograms at 20 mV s^{-1}.

As seen from Fig. 5.5, the effect of Pt catalyst slowly weakens, as the cycles of the cyclic voltammetry grows, which means the durability of the catalyst is relatively acceptable.

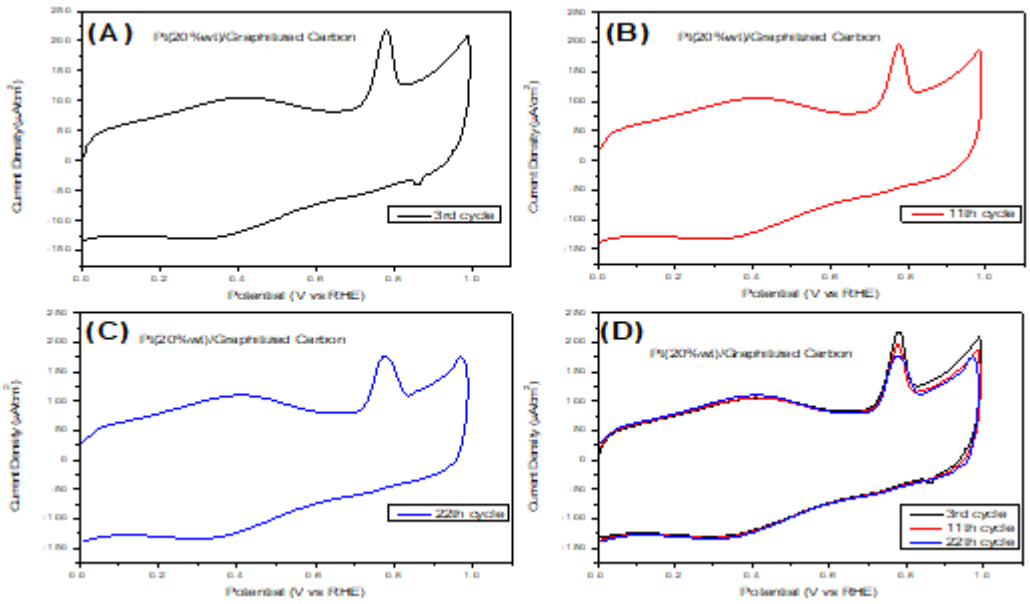

Figure 5.5. Electrochemical durability of Pt(20%wt)/graphitized carbon electrocatalyst in 0.5 mM uric acid in a 0.15 M PBS: (A) 3rd cycle, (B) 11th cycle, (C) 22th cycle (scan rate: 20 mV s^{-1}, 26 ^{o}C). (D): Comparison of all the previous cycles.

Furthermore, chronoamperometry tests were executed in order to observe the stability and possible poisoning of the Pt(20%wt)/graphitized carbon under short time continuous

operation. The operation took place for 4000 s at a constant applied potential of 0.75 V (vs Ag/AgCl), as portrayed at Fig. 5.6. It is observed that the current density increases with the raise of temperature, while the current density decreases abruptly with time, following a parabolic path and then reaches a pseudo steady-state within 320 seconds.

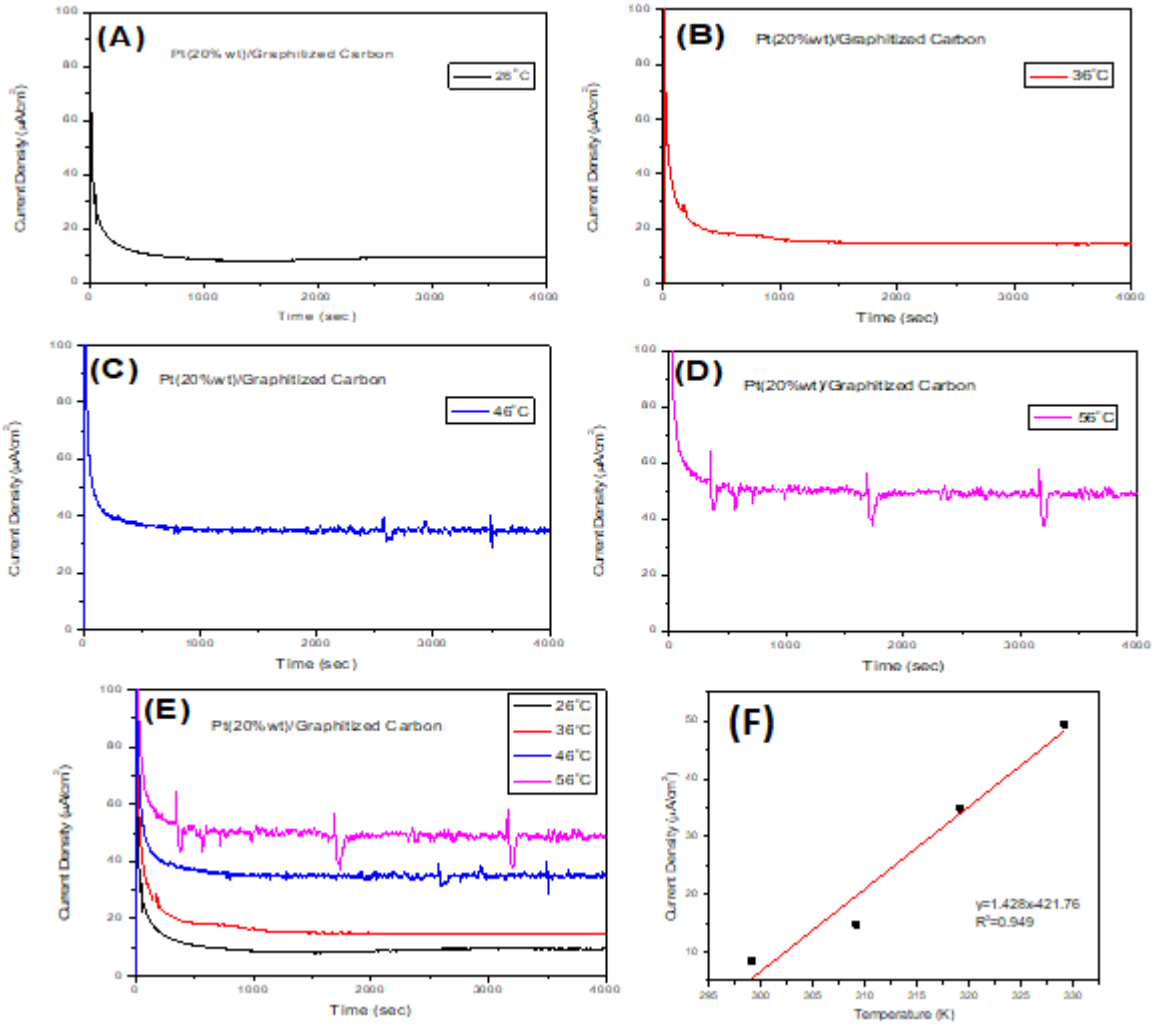

Figure 5.6. Chronoamperometric curves of Pt(20%wt)/graphitized carbon electrocatalyst at 0.75 V (vs Ag/AgCl) for 4000 sec, in 0.5 mM uric acid in a 0.15 M PBS at different temperature values: (A) 26 ºC, (B) 36 ºC, (C) 46 ºC, (D) 56 ºC, (scan rate 20 mV s^{-1}); (E): Comparison of all previous chronoamperometric curves. (F): Relationship between current density and temperature.

The poisoning rate (d) obeys the following equation[122]:

$$\delta = \frac{100}{\mathrm{I}_o}\left(\frac{d\mathrm{I}}{dt}\right)_{t \succ 500s} \qquad (5.2)$$

where I_0 is the current at the start of polarization back extrapolated from the linear current decay and $\left(\frac{d\mathrm{I}}{dt}\right)_{t \succ 500s}$ is the slope of the linear portion of current decay. From the previous equation (5.2), the poisoning rate cam be calculated to be 0.00542, 0.0064, 0.00249, 0.00104 % s^{-1} at 26°C, 36 °C, 46 °C and 56 °C, respectively.

Cyclic voltammetry and chronoamperometry experiments were carried out in order to confirm whether Pt(20%wt)/graphitized carbon electrocatalyst is able to detect ascorbic acid. Cyclic voltammetry was performed using 0.15 M PBS in absence and in presence of 0.5 mM ascorbic acid in order to determine where the AA oxidation takes place. It is clearly shown in Fig.5.7 that the oxidation occurs at 0.43 V, while the reduction at 0.23 V.

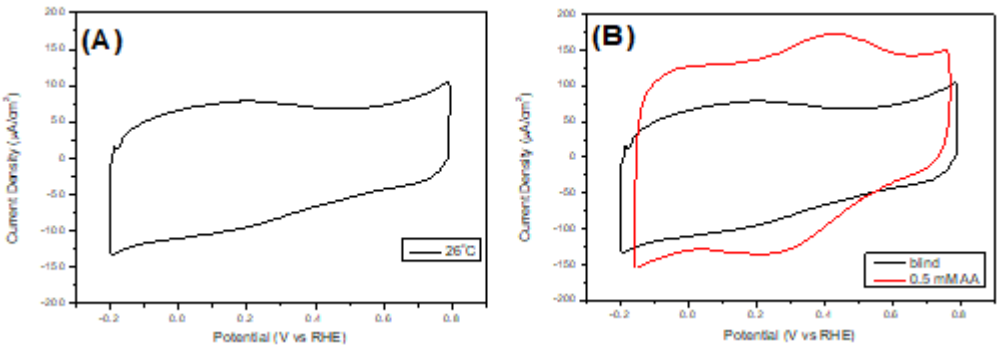

Figure 5.7. Cyclic voltammograms of the Pt(20%wt)/graphitized carbon in: (A) 0.15 M PBS and (B) 0.5 mM ascorbic acid in a 0.15 M PBS (scan rate: 20 mV s^{-1}, 26 °C).

There are many reports in literature in which the oxidation of ascorbic acid is determined, using modified electrodes. For example, *p*-aminophenol modified carbon nanotubes paste electrode (APMCNTPE) was used in order to examine the electro-catalytic oxidation of ascorbic acid. Using cyclic voltammetry the anodic peak potential is at 0.32 V, which is close to 0.43 V [14]. Similar to this work is a Ag based electro-catalyst with a peak potential at 0.37V and wide linear range of 0.17 μM to 1.80 mM, with a detection limit of

approximately 0.06 μM [13]. Another work is about a Pt modified electrode, which exhibited a good ascorbic acid electro-catalytic oxidation activity in 0.1 M KH_2PO_4, using cyclic voltammetry. The anodic current peak is about 13.67 μA while the peak potential is around 0.2 V. [11].

Table 5-2: Comparison of modified electrodes in the literature with this work.

Working Electrode	Reference Electrode	Methods	Concetration Range (mM)	Peak Potential(V)	Detection Limit(mM)	Refs
DL-Ala/Pt	Ag/AgCl	CV,CA	2-7.5	0.2	9.24	[11]
branch-trunk Ag	Ag/AgCl	CV, CA	0.17-1.80	0.37	0.06	[13]
APMCNTPE	Ag/AgCl	CV, DPV	0.2-12	0.32	0.08	[14]
Pt/C/GCE	RHE	CV, CA	0.5	0.43	-	This work

The following figure (Figs 5.8) presents the cyclic voltammetric curves for ascorbic acid in PBS, 7.3pH in order to investigate the effect of temperature on the oxidation of ascorbic acid. These four temperature values are 26ºC, 36ºC, 46ºC and 56ºC. The current density values are found to be 173.7 μA cm^{-2}, 188.5 μA cm^{-2}, 207.9 μA cm^{-2} and 261.8 μA cm^{-2} at 26 ºC, 36 ºC, 46 ºC and 56 ºC, respectively. Also, as the temperature of the solution is increased, the peak current is raised as well, demonstrating the increase of the kinetic energy of the ascorbic acid molecules, confirming the dependence of the peak current from temperature. These data illustrate that Pt(20%wt)/graphitized carbon is suitable for ascorbic acid sensing.

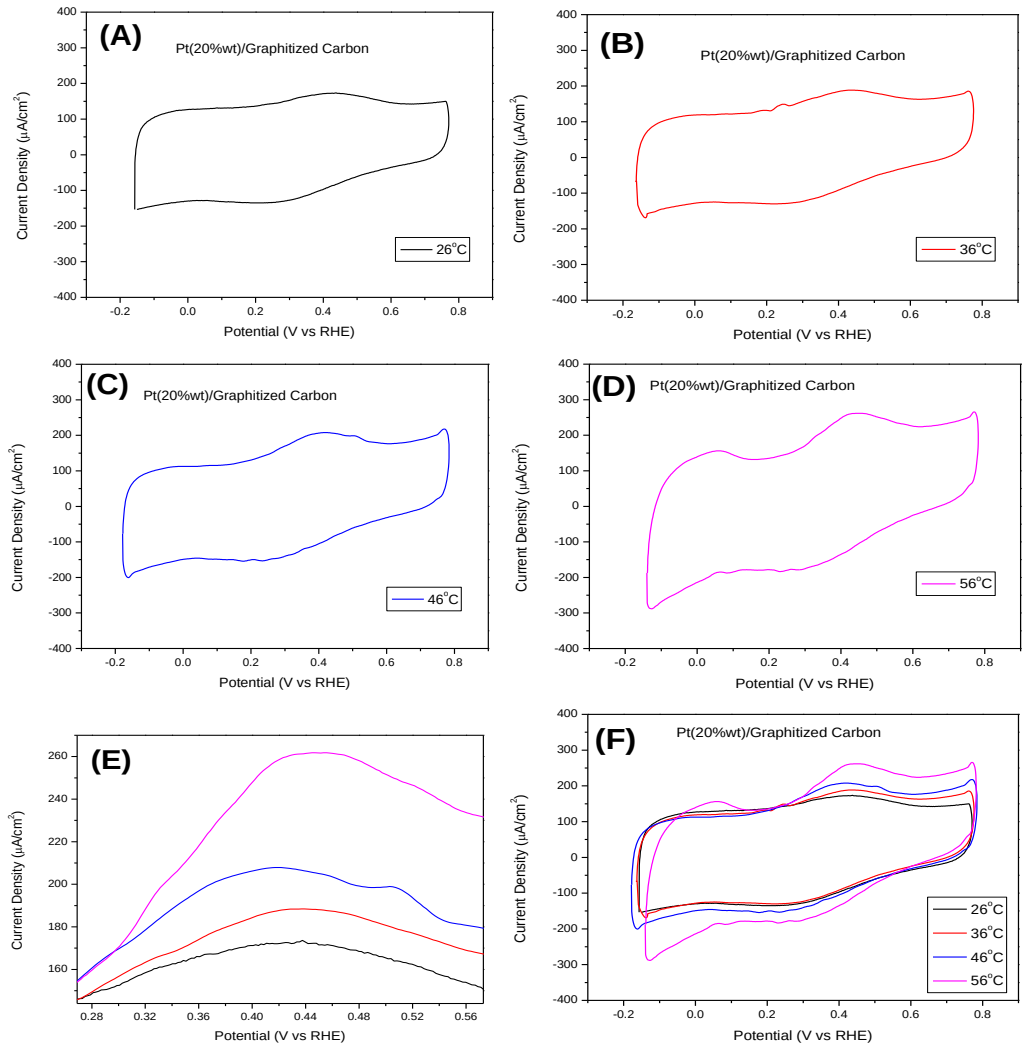

Figure 5.8. Cyclic voltammograms of Pt(20%wt)/graphitized carbon electrocatalyst in 0.5 mM ascorbic acid in a 0.15 M PBS at: (A) 26 ºC, (B) 36 ºC, (C) 46 ºC, (D) 56 ºC, (scan rate 20 mV s^{-1}). (E): Focus on the oxidation peak current. (F): Comparison of all previous cyclic voltammograms.

Using the equation (5.1) and the Fig. 5.9 the activation energy is calculated at 10.89 $kJmol^{-1}$ and it can be observed that the value of activation energy is satisfying [123].

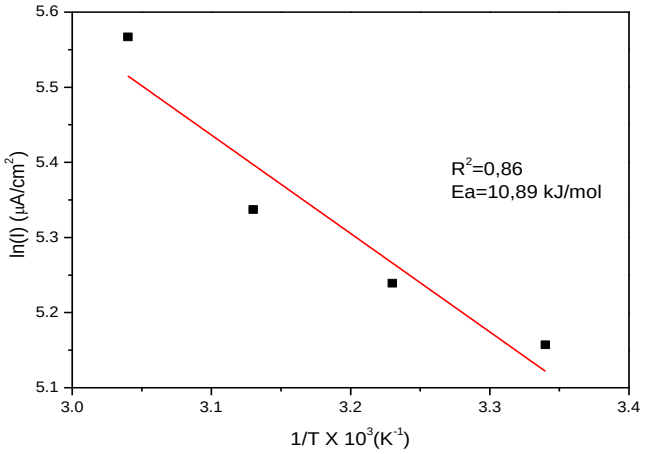

Figure 5.9. Arrhenius plot for the Pt(20%wt)/graphitized carbon electrocatalyst in 0.5 mM ascorbic acid in a 0.15 M PBS derived from cyclic voltammograms at 20 mV s^{-1}.

As seen from Fig. 5.10 the effect of the Pt catalyst remains stable as the cycles of the cyclic voltammetry increases, which establishes that the catalyst demonstrated great durability.

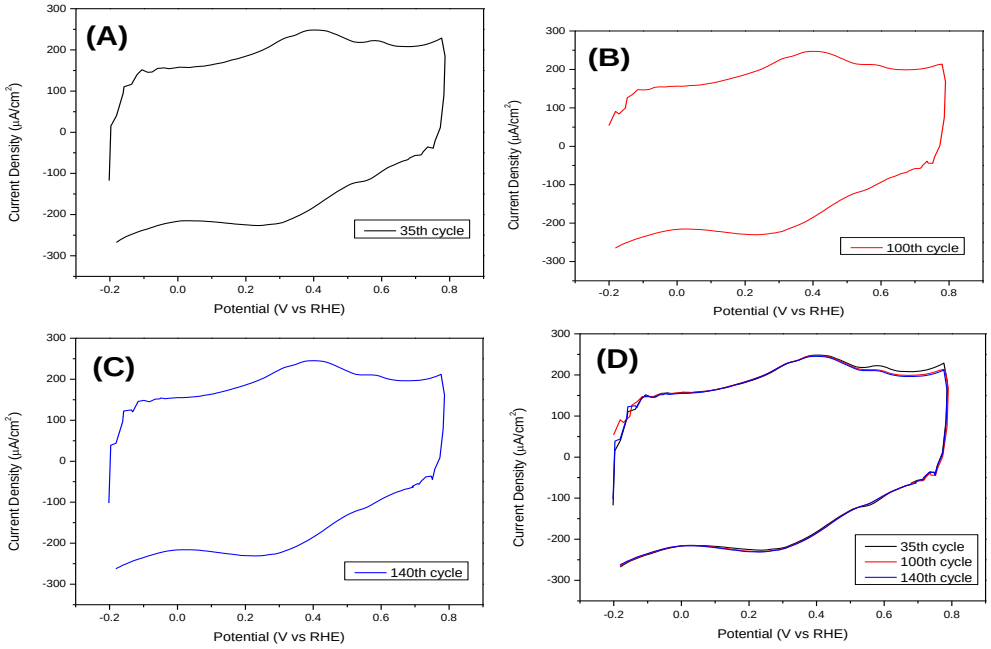

Figure 5.10. Electrochemical durability of Pt(20%wt)/graphitized carbon electrocatalyst in 0.5 mM ascorbic acid in a 0.15 M PBS: (A) 35th cycle, (B) 100th cycle, (C) 140th cycle (scan rate 20 mV s^{-1}, 26 ^{o}C). (D): Comparison of all the previous cycles.

The stability of the manufactured sensor was also tested with chronoamperometry for 4000 seconds (Fig 5.11) at a constant applied potential of 0.49 V (vs Ag/AgCl). As it should be, the current density increases as temperature rises.

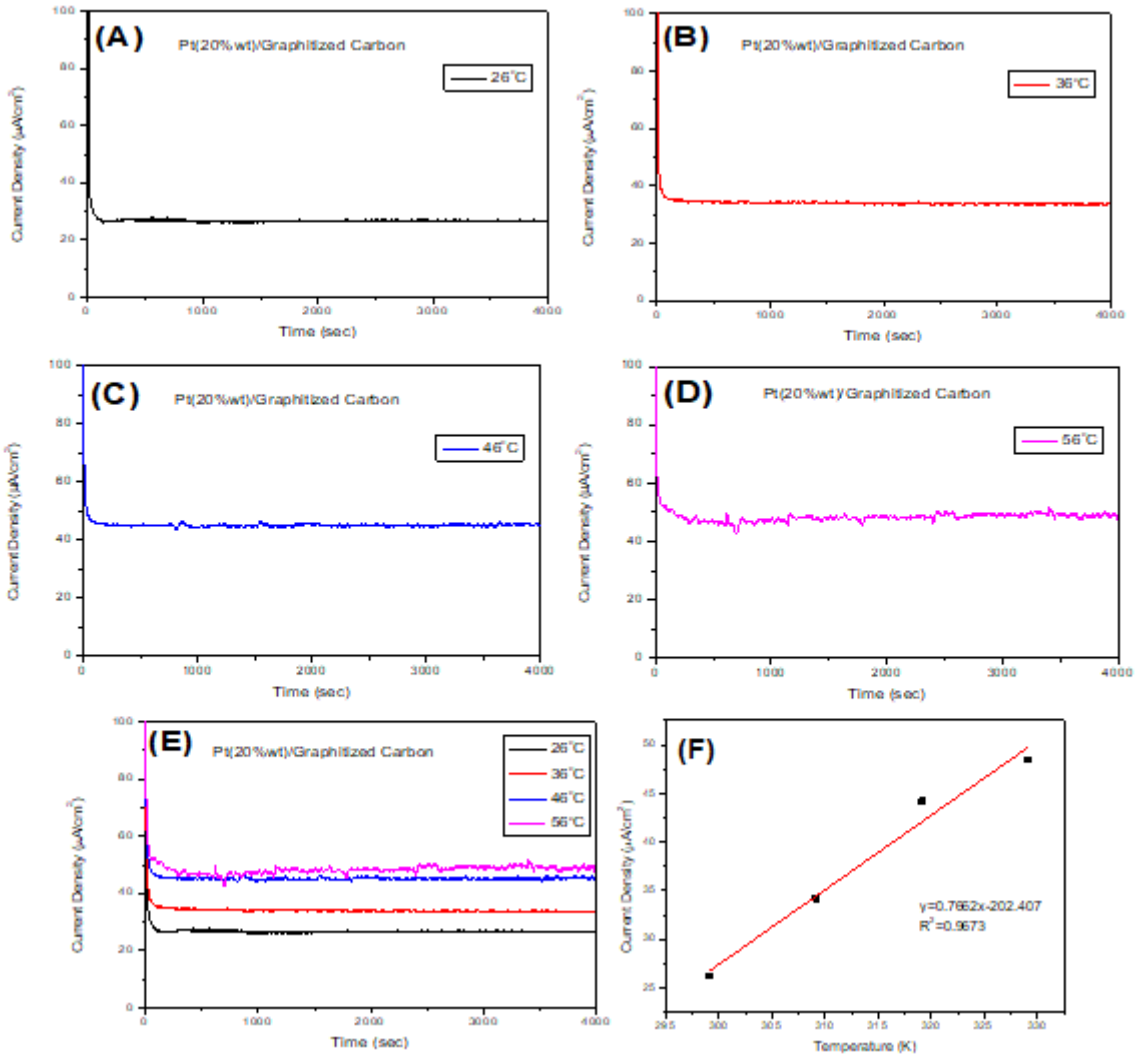

Figure 5.11. Chronoamperometric curves of Pt(20%wt)/graphitized carbon electrocatalyst at 0.49 V (vs Ag/AgCl) for 4000 sec, in 0.5 mM ascorbic acid in a 0.15 M PBS at different temperature values :(A) 26ºC, (B) 36ºC, (C) 46ºC, (D) 56ºC, (20 mV s^{-1}), (E): Comparison of all previous chronoamperometric curves. (F): Relationship between current density and temperature.

The poisoning rates at 26 ºC, 36 ºC, 46 ºC and 56 ºC are calculated taking into consideration the equation (5.2) and are calculated to be 0.00225, 0.00029, 0.00139 and

0.00014 % s^{-1}, respectively. Unfortunately, exhibiting low susceptibility to poisoning at all temperatures and potentials and the significant lower sensitivity of this catalyst prevented the execution of a successful sensitivity test.

5.2 Pd (20%wt)/Vulcan-XC72 electrocatalyst

In the chapter, the results of the physicochemical and electrochemical characterization of the commercial Pd(20wt%)/Vulcan-XC72 for uric and ascorbic acid electro-oxidation are presented. More precisely, the catalyst structure was characterized by transmission electron microscopy (TEM). The electrochemical characterization conducted via cyclic voltammetry (CV) and chronoamperometry (CA) and rotating disk electrode (RDE).

5.2.1 Physicochemical characterization

The morphology of the surface of the Pd(20wt%)/Vulcan-XC72 prepared catalyst was also examined by TEM. TEM images in Fig 5.12.a and Fig 5.12.b demonstrate a successful loading dispersion of Pd/C nanoparticles onto the surface of carbon substrate [124].

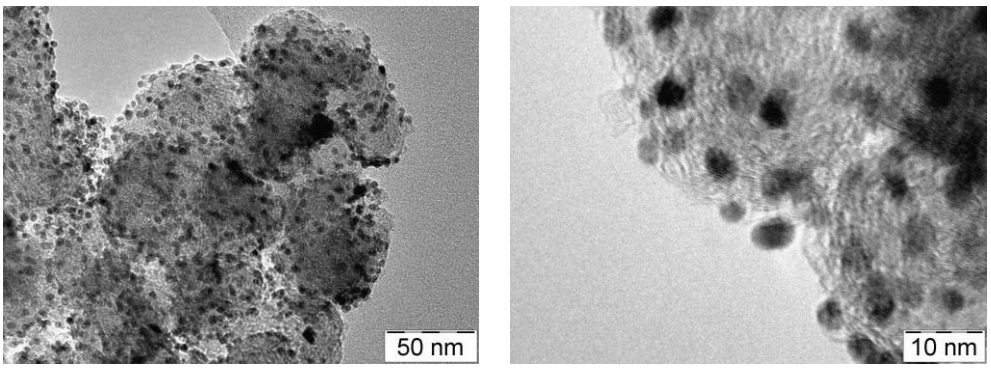

Figure 5.12. TEM images of Pd(20wt%)/Vulcan-XC72.

5.2.2 Electrochemical characterization

The electrochemical detection of uric acid was investigated by cyclic voltammetry and the stability and poisoning rate during time by chronoamperometry. All cyclic voltammetries conducted at 20mV s^{-1} scan rate, with open circuit voltage at 0.23 V (Fig. 5.13). The oxidation of uric acid is not clearly shown in the cyclic voltammogram but there is an

assumption that occurs from 0.7 to 0.85 V, whereas the reduction is clearly shown at 0.54V. The cathodic peak current is much easier found, with the maximum value at -142 μA cm^{-2}. It can be found in the literature that other Pd based electro-catalysts exhibit better oxidation peaks. Pd_3Pt_1/PDDA-RGO nanomaterials and Palladium nanoparticle-loaded carbon nanofibers (Pd/CNFs) used to detect uric acid by cyclic voltammetry is a great example [37, 125] .

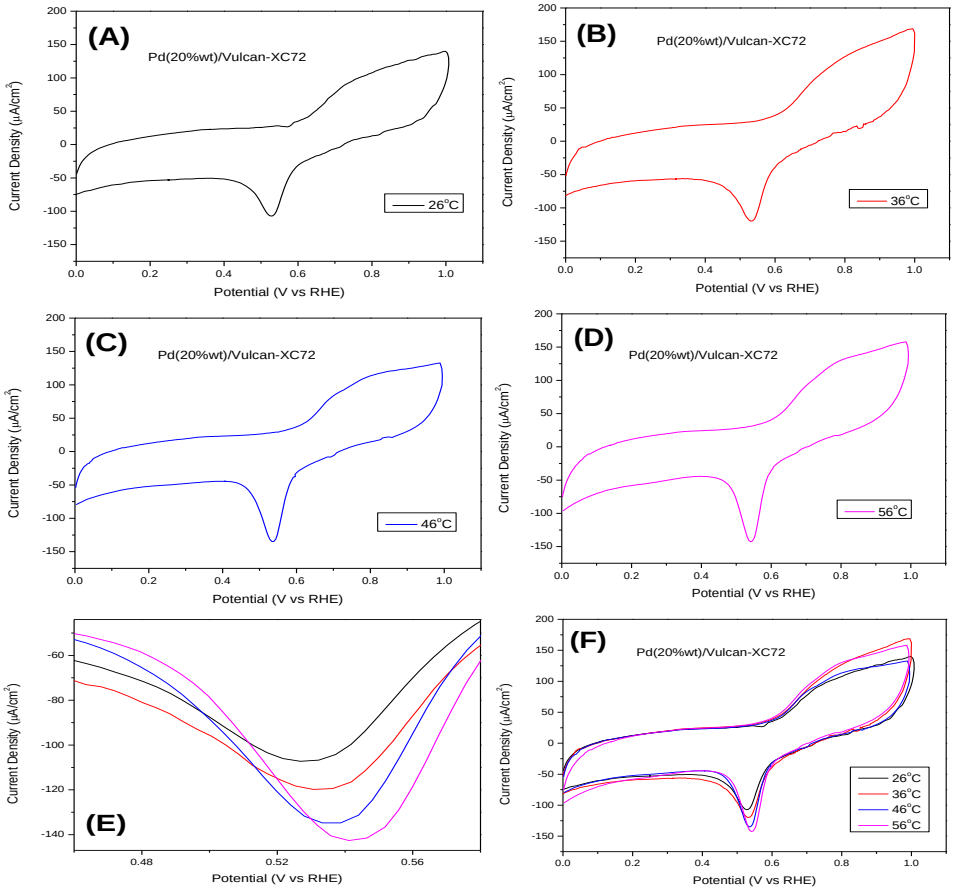

Figure 5.13. Cyclic voltammograms of Pd(20%wt)/Vulcan-XC72 electrocatalyst in 0.5 mM uric acid in a 0.15 M PBS at: (A) 26 ºC, (B) 36 ºC, (C) 46 ºC, (D) 56 ºC, (20 mV s^{-1}). (E): Focus on the reduction peak current. (F): Comparison of all previous cyclic voltammograms.

In Fig. 5.14 presents the durability of the electro-catalyst is investigated. The stable duration of it is very low, due to the oxidation and the reduction peak current decreasing with time.

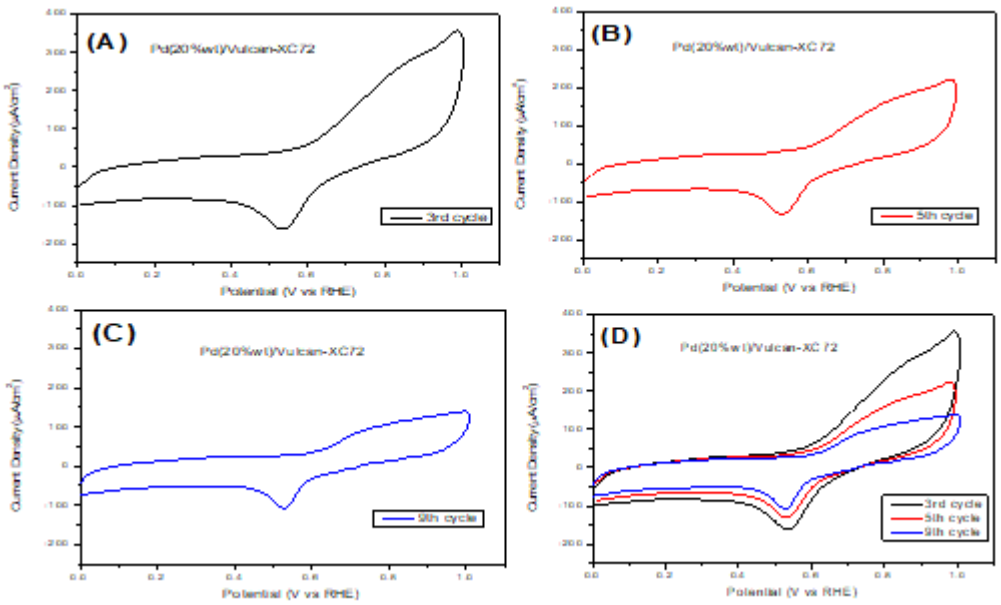

Figure 5.14. Electrochemical durability of Pd(20%wt)/Vulcan-XC72 electrocatalyst in 0.5 mM uric acid in a 0.15 M PBS: (A) 3rd cycle, (B) 5th cycle, (C) 9th cycle (scan rate 20 mV s^{-1}, 26 ºC). (D): Comparison of all the previous cycles.

Chronoamperometry technique was also used in order to evaluate the performance, the stability and the poisoning rate of the Pd(20%wt) on glassy carbon electrode of 0.5 mM uric acid in physiological buffer solution at 0.6 V (vs Ag/AgCl). This method lasted 4000s and according to Fig. 5.15 it was found that the current density decreases abruptly with time, following a parabolic path and then reaches a pseudo steady-state within 250 s. Lastly, the poisoning rate was measured from the equation (5.2) and found to be 0.003, 0.0009, 0.001, 0.00104 % s^{-1} at 26ºC, 36 ºC, 46 ºC and 56 ºC, respectively.

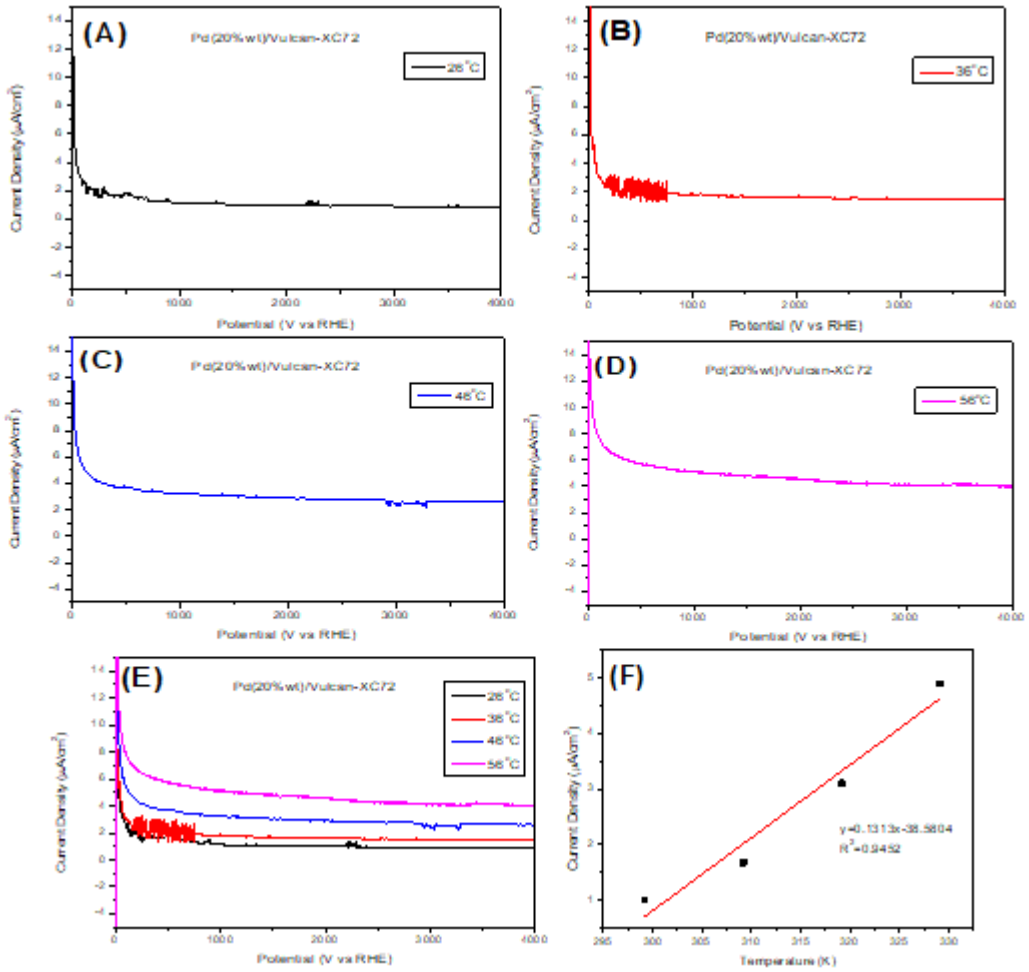

Figure 5.15. Chronoamperometric curves of Pd(20%wt)/Vulcan-XC72 electrocatalyst at 0.65 V (vs Ag/AgCl) for 4000 sec, in 0.5 mM uric acid in a 0.15 M PBS at different temperature values: (A) 26 ºC, (B) 36 ºC, (C) 46 ºC, (D) 56 ºC, (scan rate 20 mV s^{-1}). (E): Comparison of all previous chronoamperometric curves. (F): Relationship between current density and temperature.

The electrooxidative properties of the glassy carbon electrode modified with the Pd(20%wt)/Vulcan-XC72 catalytic paste in order to detect ascorbic acid are exhibited below, with the use of cyclic voltammetry, chronoamperometry and rotating disk electrode [126]. In Fig. 5.16, the comparison between the cyclic voltammograms of the Pd(20%wt)/Vulcan-XC72 in 0.15 M PBS in absence and in presence of 0.5 mM ascorbic acid, indicate two peaks. The first is around -0.04 V, which is explained by hydrogen

absorption. The second one at 0.43 V, due possibly to the ascorbic acid oxidation, although, our experimental results are not enough to give an absolute answer. From literature information it is found that Palladium nanoparticle-loaded carbon nanofibers (Pd/CNFs) used for CV detection of ascorbic acid, exhibited the oxidation peak potential at 0.465 V; almost the same with the present work [125].

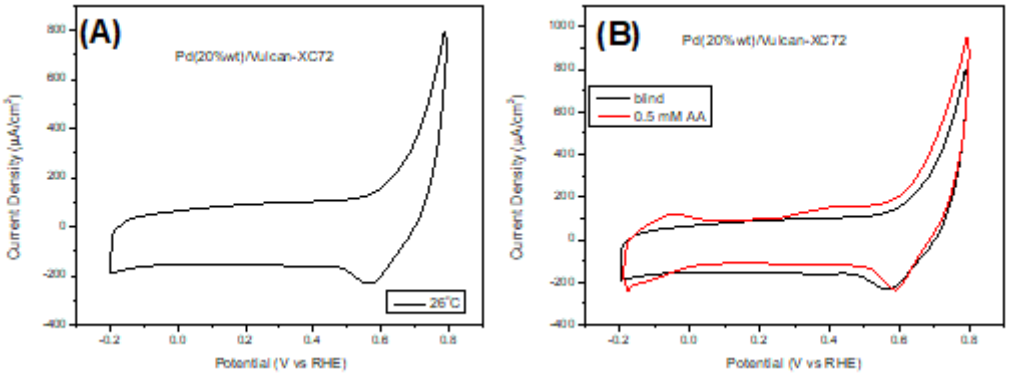

Figure 5.16. Cyclic voltammograms of the Pd(20%wt)/Vulcan-XC72 in:(A) 0.15 M PBS, (B) 0.5 mM ascorbic acid in a 0.15 M PBS (scan rate 20 mV s^{-1}, 26 ^{o}C).

The figure below (Fig 5.17) shows the cyclic voltammetric curves for oxidation of 0.5 mM ascorbic acid in 0.15 M PBS, 7.3 pH, at the temperature values of 26^{o}C, 36^{o}C, 46^{o}C and 56 ^{o}C and the scan rate was 20 mV/s; the corresponding peak current density values are found to be 125.9 μA cm^{-2}, 150.6 μA cm^{-2}, 181.3 μA cm^{-2} and 185.5 μA cm^{-2}. The increase of peak current density values with temperature could be attributed to the increase of the kinetic energy of the ascorbic acid molecules, confirming the dependence of the peak current from temperature.

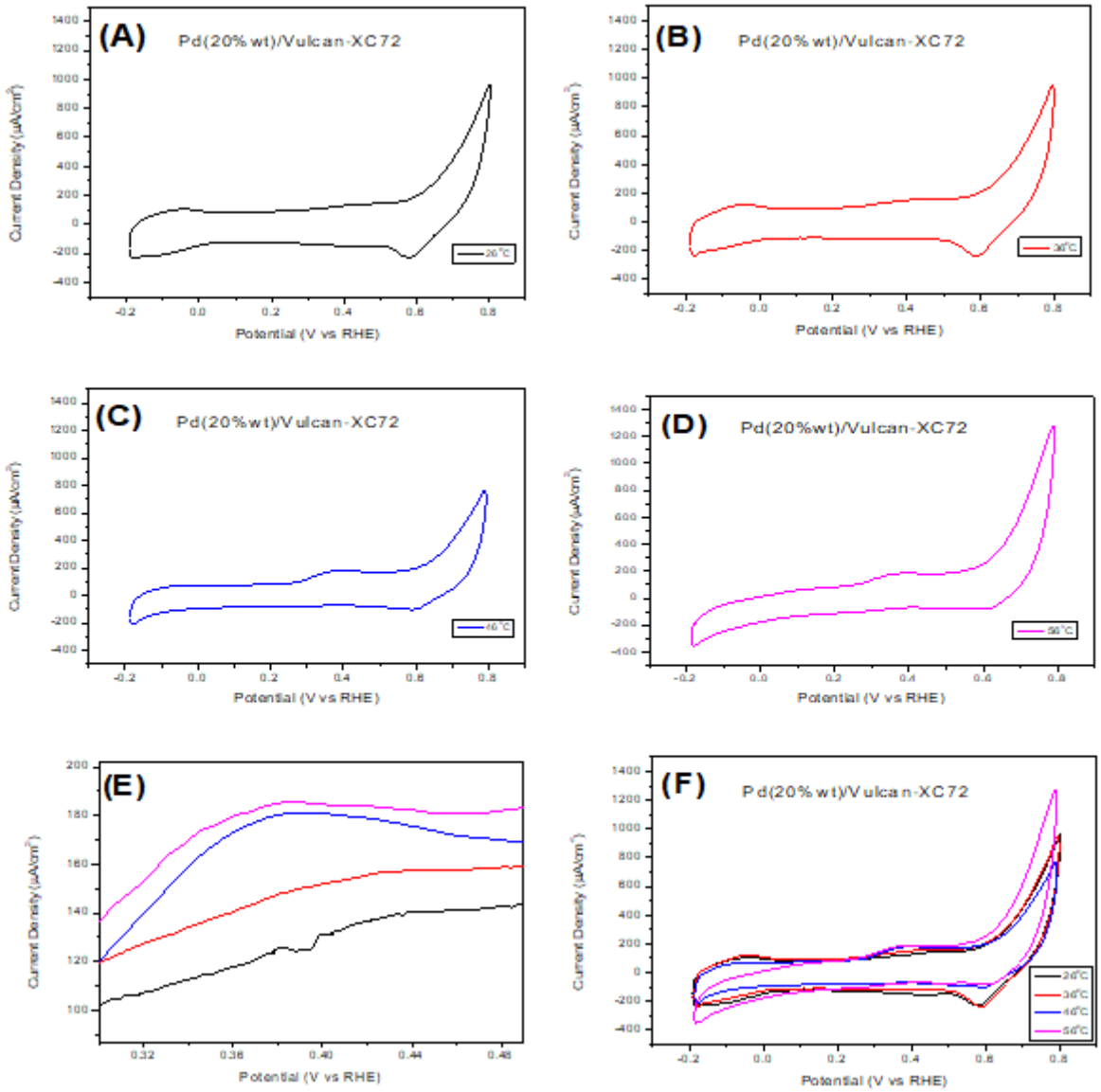

Figure 5.17. Cyclic voltammograms of Pd(20%wt)/Vulcan-XC72 electrocatalyst in 0.5 mM ascorbic acid in a 0.15 M PBS at: (A) 26 ºC, (B) 36 ºC, (C) 46 ºC, (D) 56 ºC, (scan rate 20 mV s^{-1}). (E): Focus on the oxidation peak current. (F): Comparison of all previous cyclic voltammograms.

Using the equation (5.1) and the Fig.5.18 (below) the activation energy is calculated to be at 11.33 kJ mol^{-1} and it can be observed that the value of activation energy is positively good [123].

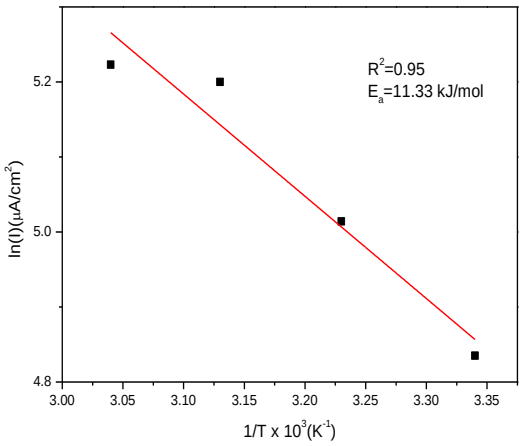

Figure 5.18. Arrhenius plot for the Pd(20%wt)/Vulcan-XC72 electrocatalyst in 0.5 mM ascorbic acid in a 0.15 M PBS derived from cyclic voltammograms at 20 mV s^{-1}.

As seen from Fig. 5.19 the effect of the Pd(20%wt)/Vulcan-XC72 catalyst also clearly decreases as the cycles of the cyclic voltammetry increase. The durability of the catalyst is comparatively low.

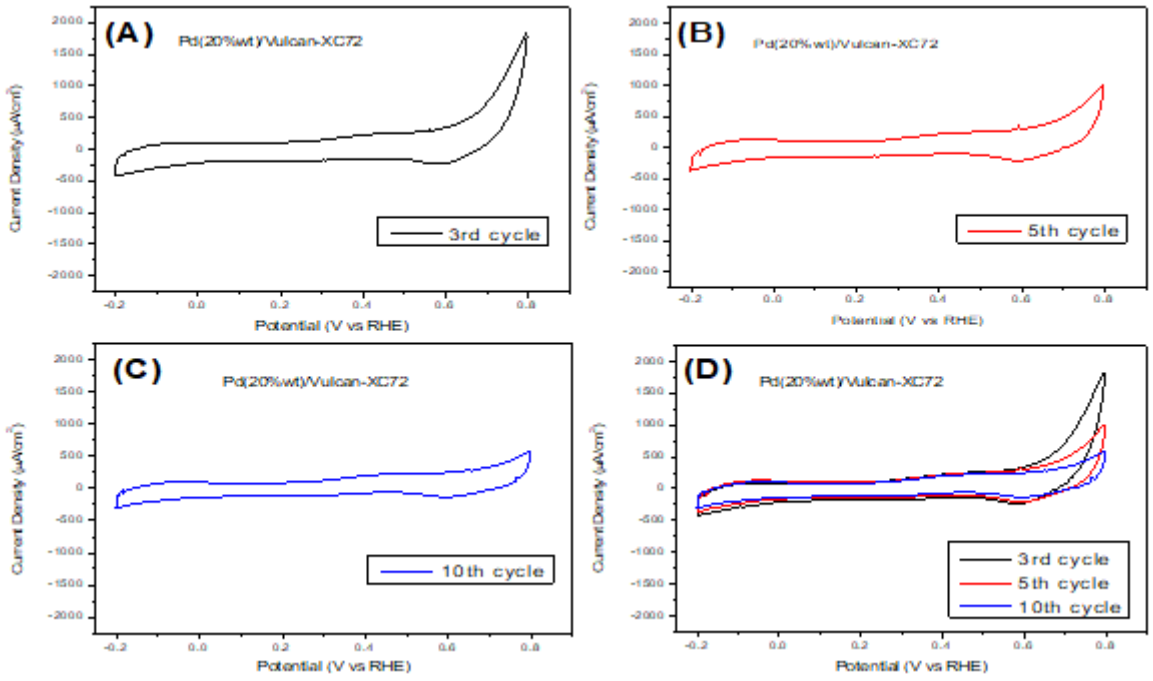

Figure 5.19. Electrochemical durability of Pd(20%wt)/Vulcan-XC72 electrocatalyst in 0.5 mM ascorbic acid in a 0.15 M PBS: (A) 3rd cycle, (B) 5th cycle, (C) 10th cycle (scan rate 20 mV s^{-1}, 26 ^{o}C). (D): Comparison of all the previous cycles.

Chronoamperometric experiments took place in order to observe the stability of the manufactured sensor (Fig. 5.20). Chronoamperometry executed for 4000 seconds at a constant applied potential of 0.29 V (vs Ag/AgCl). As expected, the current density increases as temperature rises. The poisoning rate at 26 ^{o}C, 36 ^{o}C, 46 ^{o}C and 56 ^{o}C, using the equation (5.2) are 0.00041, 0.0003, 0.0007 and 0.00055 % s^{-1}, respectively. These values demonstrate low susceptibility to poisoning at all temperatures.

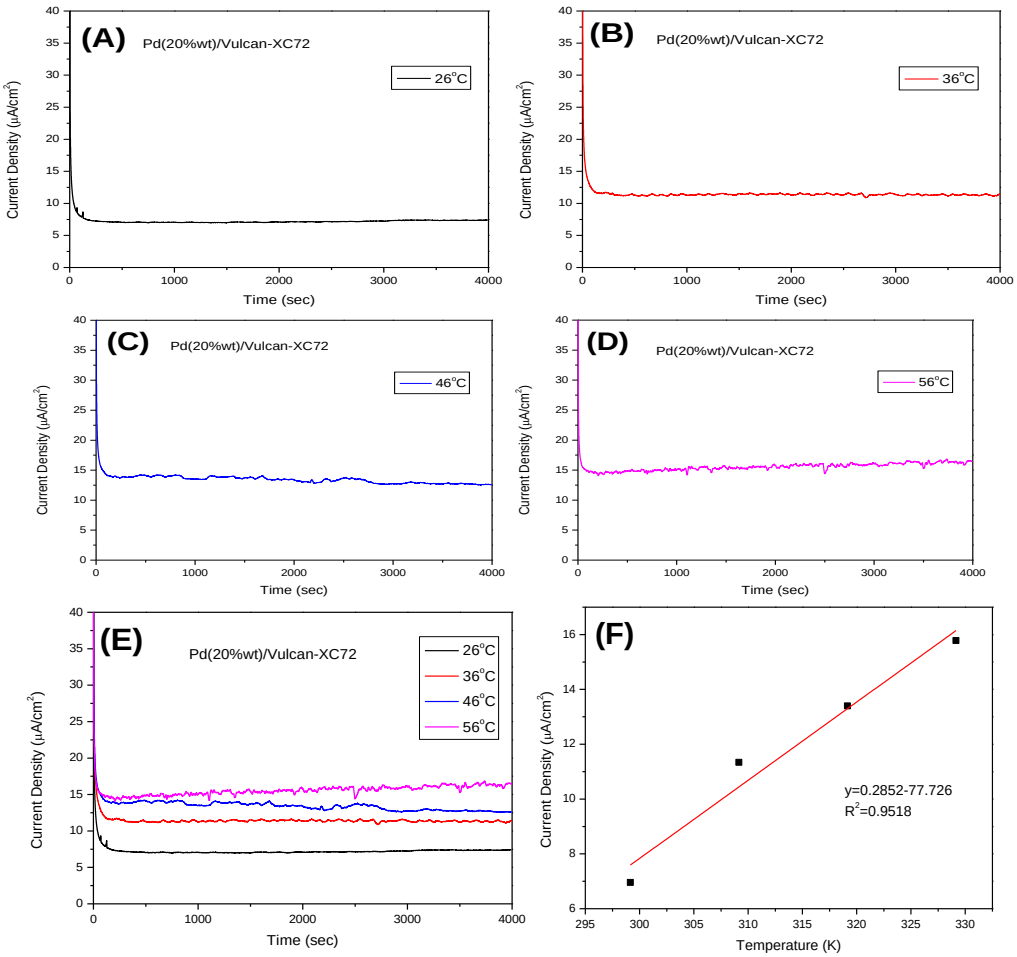

Figure 5.20. Chronoamperometric curves of Pd(20%wt)/Vulcan-XC72 electrocatalyst at 0.29V (vs Ag/AgCl) for 4000sec, in 0.5 mM ascorbic acid in a 0.15 M PBS at different temperature values :(A) 26 ^{o}C, (B) 36 ^{o}C, (C) 46 ^{o}C, (D) 56 ^{o}C, (scan rate 20 mV s^{-1}). (E): Comparison of all previous chronoamperometric curves. (F): Relationship between current density and temperature.

A successful sensitivity test is also completed with the Pd(20%wt)/Vulcan-XC72 catalytic paste, with the use of a rotating disk electrode, as presented in the figure below (Fig 5.21):

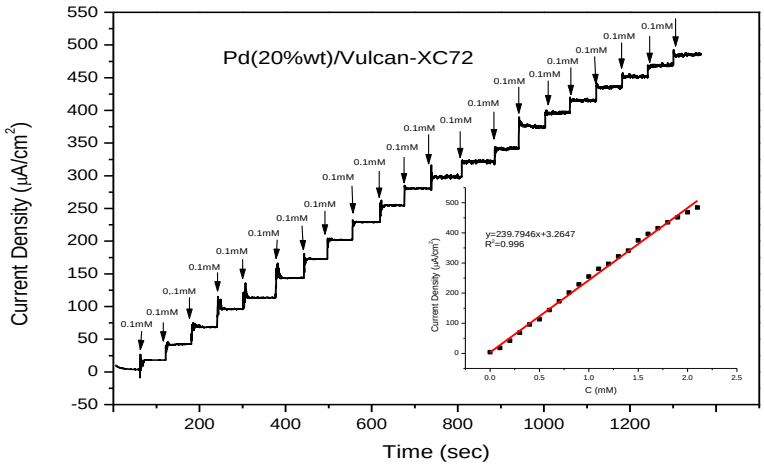

Figure 5.21. Current-time record of Pd(20%wt)/Vulcan-XC72, 1600rpm**.**

This figure is a current–time record of Pd(20%wt)/Vulcan-XC72 catalyst deposited onto rotating disk electrode at 1600 rounds per minute, by successively injection 0.1 mM AA each time into physiological buffer solution at a regular interval time of 50 s [127]. The experiment was conducted at 0.4 V applied potential. Inset is the relationship between the current density and the added ascorbic acid solution. Pd(20%wt)/Vulcan-XC72 showed great sensitivity to the changes of the concentration of ascorbic acid at the solution.

CHAPTER 6: Conclusions and future perspectives

The activity of Pt(20%wt)/graphitized carbon and Pd(20%wt)/Vulcan-XC72 catalyst towards the electro-oxidation of 0.5 mM ascorbic and uric acid in physiological-buffered solution of 7.3 pH was demonstrated using fundamental electrochemical techniques. Cyclic voltammetry and chronoamperometry experiments on glassy carbon electrode coated with Pd(20%wt)/Vulcan-XC72 and Pt(20%wt)/graphitized carbon exhibited interesting results for the detection of ascorbic and uric acid. Initially, cyclic voltammetries of 0.15 M PBS with and without the presence of ascorbic or uric acid was examined, in order to evaluate the activity of each catalyst. Afterwards, the effect of temperature, the durability, the stability and the sensitivity of each electrocatalyst was investigated.

From the cyclic voltammograms of the Pt(20%wt)/graphitized carbon in 0.15 M PBS, 0.15 M PBS with 0.5 mM uric acid and 0.15 M PBS with 0.5 mM ascorbic acid, the oxidation of each compound was established successfully. At 26 ^{o}C the anodic current peak for uric acid was 193.2 μA cm^{-2} at 0.79 V and for ascorbic acid was 173.7 μA cm^{-2} at 0.43 V. By applying different temperatures, the anodic current peaks were constantly increased with the rise of temperature. From these results, activation energy was calculated at 31.8 kJ mol^{-1} and 10.89 kJ mol^{-1} for uric and ascorbic acid, respectively. The catalyst exhibited great durability towards the ascorbic acid solution, in contrast to the uric acid mixture, which lost its durational properties after the 11^{th} cycle. Finally, in each solution the poisoning rate of the catalyst was relatively low.

As for Pd(20%wt)/Vulcan-XC72, the cyclic voltammetry in 0.15 M PBS, 0.5 mM uric acid in 0.15 M PBS and 0.5 mM ascorbic acid in 0.15 M PBS demonstrated negligible results that indicated minor oxidative properties. Anodic current peaks were increased as the temperature escalated. The oxidation of ascorbic acid at 26 ^{o}C resulted to an anodic current peak current of 125 μA cm^{-2} at 0.43 V and at the durability experiment the catalyst displayed poor quality. However, a successful sensitivity test was conducted. The catalytic

activity at the uric acid solution was unable to be determined, because the anodic current peak could not be distinguished. Therefore, more experiments should take place.

Pt(20wt%)/graphitized carbon presented better electrochemical activity and durability than Pd(20%wt)/Vulcan-XC72, which is shown clearly by the cyclic voltammograms. On the other hand, Pd(20%wt)/Vulcan-XC72 demonstrated great sensitivity towards ascorbic acid. In each case, the poisoning rate of all chronoamperometry curves were relatively low, which established satisfying stability and the anodic current peaks were constantly increased with the rise of temperature.

As for future perspectives the effect of various concentrations, pH, pressure levels and scan rate could be examined. Furthermore, the simultaneous detection of ascorbic and uric acid is certainly a valuable study. Simultaneous determination of ascorbic and uric acid can be executed with the use of the differential pulse voltammetry technique.

References

[1] K. Iqbal, A. Khan and M.M.A.K.J.P.J.o.N. Khattak, 3 (2004) 5.
[2] J.J.T.A.j.o.m. Burns, 26 (1959) 740.
[3] Altervista, ISOMERIA OTTICA: Vitamina C in JSmol, Chimica in JSmol, 2013.
[4] B. Sunil Kumar, S. Singh, R.J.C.r.i.f.s. Verma and nutrition, 57 (2017) 2623.
[5] Y. Ma, J. Chapman, M. Levine, K. Polireddy, J. Drisko and Q.J.S.t.m. Chen, 6 (2014) 222ra18.
[6] S.J. Padayatty, H.D. Riordan, S.M. Hewitt, A. Katz, L.J. Hoffer and M.J.C.M.A.J. Levine, 174 (2006) 937.
[7] C.R. Mayland, M.I. Bennett and K.J.P.m. Allan, 19 (2005) 17.
[8] E. Klimant, H. Wright, D. Rubin, D. Seely and M.J.C.O. Markman, 25 (2018) 139.
[9] A. Pardakhty, S. Ahmadzadeh, S. Avazpour and V.K.J.J.o.M.L. Gupta, 216 (2016) 387.
[10] J. Lavanya and N.J.T. Gomathi, 144 (2015) 655.
[11] H. Rageh, M. Abou-Krisha, A. Abo-Bakr and M.J.I.J.E.S. Abd-Elsabour, 10 (2015) 4105.
[12] F. Yang, J. Wang, Y. Cao, L. Zhang, X.J.S. Zhang and A.B. Chemical, 205 (2014) 20.
[13] Y. Zhang, P. Liu, S. Xie, M. Chen, M. Zhang, Z. Cai, R. Liang, Y. Zhang and F.J.J.o.E.C. Cheng, 818 (2018) 250.
[14] S. Gheibi, H. Karimi-Maleh, M.A. Khalilzadeh, H.J.J.o.F.S. Bagheri and Technology, 52 (2015) 276.
[15] S. Hameed, A. Munawar, W.S. Khan, A. Mujahid, A. Ihsan, A. Rehman, I. Ahmed, S.Z.J.B. Bajwa and Bioelectronics, 89 (2017) 822.
[16] J. Sui, W. Li and Q.J.J.o.M.S. Pan, Part B, 56 (2017) 623.
[17] C. van der Horst, B. Silwana, E. Iwuoha, E. Gil and V.J.F.A.M. Somerset, 9 (2016) 2560.
[18] M.A. Wahab, F. Darain, N. Islam and D.J.J.M. Young, 23 (2018) 234.
[19] V. Arabali, M. Ebrahimi, M. Abbasghorbani, V.K. Gupta, M. Farsi, M. Ganjali and F.J.J.o.M.L. Karimi, 213 (2016) 312.
[20] L. Fu, Y.-H. Zheng and Z.-X.J.C.P. Fu, 69 (2015) 655.
[21] M. Bijad, H. Karimi-Maleh and M.A.J.F.A.M. Khalilzadeh, 6 (2013) 1639.
[22] H. Beitollahi, S. Tajik, H. Parvan, H. Soltani, A. Akbari and M.H.J.A.B.E. Asadi, 6 (2014) 54.
[23] S. Watanabe, D.-H. Kang, L. Feng, T. Nakagawa, J. Kanellis, H. Lan, M. Mazzali and R.J.J.H. Johnson, 40 (2002) 355.
[24] C.E. Markowitz, S. Spitsin, V. Zimmerman, D. Jacobs, J.K. Udupa, D.C. Hooper, H.J.T.J.o.A. Koprowski and C. Medicine, 15 (2009) 619.
[25] A. Busch and T. Stief, Taurine strongly enhances the ROS generation of blood neutrophils, 2013.

[26] G. Mossetti, D. Rendina, G. De Filippo, D. Benvenuto, C.L. Vivona, G. Zampa, P. Ferraro, P.J.C.c.i.m. Strazzullo and b. metabolism, 5 (2008) 114.
[27] N. Papanas, N. Katsiki, K. Papatheodorou, M. Demetriou, D. Papazoglou, T. Gioka and E.J.A. Maltezos, 62 (2011) 291.
[28] A. Abraham, H. Albulaihe, M. Alabdali, M. Qrimli, A. Breiner, C. Barnett, H.D. Katzberg, L.E. Lovblom, B.A. Perkins, V.J.M. Bril and nerve, 53 (2016) 862.
[29] M. Moccia, R. Lanzillo, R. Palladino, C. Russo, A. Carotenuto, M. Massarelli, G. Vacca, V. Vacchiano, A. Nardone, M.J.C.C. Triassi and L. Medicine, 53 (2015) 753.
[30] M. Weisskopf, E. O'reilly, H. Chen, M. Schwarzschild and A.J.A.j.o.e. Ascherio, 166 (2007) 561.
[31] L. Xu, Y. Han, P. Li, L. Ma, Y. Xin, X. Hao, H. Huang, B. Liu and N.J.J.A.S.E.I. Yang, 4 (2017) 39.
[32] D. Lakshmi, M.J. Whitcombe, F. Davis, P.S. Sharma and B.B.J.E. Prasad, 23 (2011) 305.
[33] S. Thiagarajan and S.-M. Chen, Talanta, 74 (2007) 212.
[34] S. Zhu, H. Li, W. Niu and G. Xu, Biosensors and Bioelectronics, 25 (2009) 940.
[35] C.-L. Sun, H.-H. Lee, J.-M. Yang and C.-C. Wu, Biosensors and Bioelectronics, 26 (2011) 3450.
[36] X. Tian, C. Cheng, H. Yuan, J. Du, D. Xiao, S. Xie and M.M.F. Choi, Talanta, 93 (2012) 79.
[37] J. Yan, S. Liu, Z. Zhang, G. He, P. Zhou, H. Liang, L. Tian, X. Zhou and H. Jiang, Colloids and Surfaces B: Biointerfaces, 111 (2013) 392.
[38] Z. Bai, C. Zhou, H. Xu, G. Wang, H. Pang and H. Ma, Sensors and Actuators B: Chemical, 243 (2017) 361.
[39] J. Wang, B. Yang, J. Zhong, B. Yan, K. Zhang, C. Zhai, Y. Shiraishi, Y. Du and P. Yang, Journal of Colloid and Interface Science, 497 (2017) 172.
[40] Q. Zhu, J. Bao, D. Huo, M. Yang, C. Hou, J. Guo, M. Chen, H. Fa, X. Luo and Y. Ma, Sensors and Actuators B: Chemical, 238 (2017) 1316.
[41] D. Zhao, D. Fan, J. Wang and C.J.M.A. Xu, 182 (2015) 1345.
[42] W. Wu, H. Min, H. Wu, Y. Ding and S.J.A.L. Yang, 50 (2017) 91.
[43] A. Brouzgou, A. Podias and P.J.J.o.A.E. Tsiakaras, 43 (2013) 119.
[44] R. O'hayre, S.-W. Cha, F.B. Prinz and W. Colella, Fuel cell fundamentals, John Wiley & Sons, 2016.
[45] L.J.W.D. Herbert, (2001).
[46] Cactusbush, Familiar Batteries, 2014.
[47] F. von Sturm, Comprehensive Treatise of Electrochemistry, Springer, 1981, p. 385.
[48] G.N. Lewis and F.G.J.J.o.t.A.C.S. Keyes, 35 (1913) 340.
[49] J.-M. Tarascon and M. Armand, Materials For Sustainable Energy: A Collection of Peer-Reviewed Research and Review Articles from Nature Publishing Group, World Scientific, 2011, p. 171.
[50] C. Iwakura, Y. Fukumoto, H. Inoue, S. Ohashi, S. Kobayashi, H. Tada and M.J.J.o.p.s. Abe, 68 (1997) 301.
[51] W. Baumann and A. Muth, Batterien: Daten und Fakten zum Umweltschutz, Springer-Verlag, 2013.
[52] H. Arai and M. Hayashi, (2009).

[53] Y. She, J. Chen, C. Zhang, Z. Lu, M. Ni, P.H.-L. Sit and M.K.J.E.P. Leung, 142 (2017) 1319.
[54] Y. Liu, Q. Sun, W. Li, K.R. Adair, J. Li, X.J.G.E. Sun and Environment, 2 (2017) 246.
[55] M. Root, The TAB™ Battery Book: An In-Depth Guide to Construction, Design, and Use, New York: McGraw-Hill/TAB Electronics, 2011.
[56] P.G. Bruce, S.A. Freunberger, L.J. Hardwick and J.-M.J.N.m. Tarascon, 11 (2012) 19.
[57] J.J.J.o.T.E.S. Read, 149 (2002) A1190.
[58] Chargedevs, KAIST discovers method to extend Li-air battery life, 2013.
[59] S.W. Kim, D.H. Seo, X. Ma, G. Ceder and K.J.A.E.M. Kang, 2 (2012) 710.
[60] W. Liu, Q. Sun, Y. Yang, J.-Y. Xie and Z.-W.J.C.C. Fu, 49 (2013) 1951.
[61] C. Largeot, C. Portet, J. Chmiola, P.-L. Taberna, Y. Gogotsi and P.J.J.o.t.A.C.S. Simon, 130 (2008) 2730.
[62] G. Wang, L. Zhang and J.J.C.S.R. Zhang, 41 (2012) 797.
[63] Graphene-Info, Graphene Supercapacitors: Introduction and News, 2018.
[64] B.E. Conway, Electrochemical supercapacitors: scientific fundamentals and technological applications, Springer Science & Business Media, 2013.
[65] M. Galiński, A. Lewandowski and I.J.E.a. Stępniak, 51 (2006) 5567.
[66] P. Simon and Y. Gogotsi, Nanoscience And Technology: A Collection of Reviews from Nature Journals, World Scientific, 2010, p. 320.
[67] B. Conway, V. Birss and J.J.J.o.P.S. Wojtowicz, 66 (1997) 1.
[68] W. Sugimoto, H. Iwata, K. Yokoshima, Y. Murakami and Y.J.T.J.o.P.C.B. Takasu, 109 (2005) 7330.
[69] X. Dong, W. Shen, J. Gu, L. Xiong, Y. Zhu, H. Li and J.J.T.J.o.P.C.B. Shi, 110 (2006) 6015.
[70] C. Zhong, Y. Deng, W. Hu, J. Qiao, L. Zhang and J.J.C.S.R. Zhang, 44 (2015) 7484.
[71] K. Zeng, D.J.P.i.E. Zhang and C. Science, 36 (2010) 307.
[72] A.A. Rahim, A.S. Tijani and F.H.J.J.o.M.E. Shukri, 12 (2015) 47.
[73] T. Riedel, M. Claeys, H. Schulz, G. Schaub, S.-S. Nam, K.-W. Jun, M.-J. Choi, G. Kishan and K.-W.J.A.C.A.G. Lee, 186 (1999) 201.
[74] E. George, D.O. Rudin and J.U. Casby, Glass electrode for measuring sodium ion, Google Patents, 1958.
[75] J. Wang, Analytical electrochemistry, John Wiley & Sons, 2006.
[76] P.D. Beer, R.J. Mortimer, N.R. Stradiotto, F. Szemes and J.S. Weightman, Analytical Proceedings including Analytical Communications 1995.
[77] M. Meyerhoff and W. Opdycke, Advances in clinical chemistry, Vol. 25, Elsevier, 1986, p. 1.
[78] C.R. Martin and H.J.A.C. Freiser, 52 (1980) 562.
[79] R. Cattrall and H.J.A.C. Freiser, 43 (1971) 1905.
[80] T.J.C.O.C. Navratil, 15 (2011) 2996.
[81] R. Mukundan, E.L. Brosha and F.H.J.J.o.T.E.S. Garzon, 150 (2003) H279.
[82] P.J.C.C.A. D'Orazio, 334 (2003) 41.
[83] E. Bakker and E.J.T.T.i.A.C. Pretsch, 24 (2005) 199.

[84] C. Kollegger, P. Greiner, I. Siegl, C. Steffan, M. Wiessflecker, B. Pekec, M. Hajnsek, F. Sinner, G. Holweg, B.J.e. Deutschmann and i.E.u. Informationstechnik, 135 (2018) 83.
[85] G.D.J.J.o.p. Christian and b. analysis, 14 (1996) 899.
[86] G. Eisenman, Glass electrodes for hydrogen and other cations: principles and practice, M. Dekker, 1967.
[87] V. Smyntyna, V. Golovanov, S. Kashulis, G. Mattogno, S.J.S. Viticoli and A.B. Chemical, 19 (1994) 460.
[88] W. Qu, J.-U.J.M.S. Meyer and Technology, 8 (1997) 593.
[89] R. Nowrouzi, F. Razi, F. Rahimi and A.I.J.S.L. Zad, 11 (2013) 2015.
[90] M. Fleischer, H.J.S. Meixner and A.B. Chemical, 25 (1995) 544.
[91] A. Joshi, S. Gangal, S.J.S. Gupta and A.B. Chemical, 156 (2011) 938.
[92] R.E. Brian, Chemical Sensors and Biosensors, Chapter, 2002.
[93] D.R. Thévenot, K. Toth, R.A. Durst and G.S.J.A.L. Wilson, 34 (2001) 635.
[94] M. Mehrvar and M.J.A.s. Abdi, 20 (2004) 1113.
[95] A. Brouzgou and P.J.T.i.C. Tsiakaras, 58 (2015) 1311.
[96] Nanohub, (2017).
[97] P. Ugo and L.M.J.E. Moretto, 7 (1995) 1105.
[98] W. Gorski and J.A.J.A.C. Cox, 64 (1992) 2706.
[99] K.Z. Liu and Q.G.J.E. Wu, 4 (1992) 569.
[100] K. Itaya, I. Uchida and V.D.J.A.o.C.R. Neff, 19 (1986) 162.
[101] R.W. Murray, A.G. Ewing and R.A.J.A.C. Durst, 59 (1987) 379A.
[102] R.M.J.S. Wightman, 240 (1988) 415.
[103] R.T. Kennedy, L. Huang, M.A. Atkinson and P.J.A.c. Dush, 65 (1993) 1882.
[104] Z. Taleat, A. Khoshroo and M.J.M.A. Mazloum-Ardakani, 181 (2014) 865.
[105] J.A. McGeough, Principles of electrochemical machining, CRC Press, 1974.
[106] T. Scarazzato, D.C. Buzzi, A.M. Bernardes, J.A.S. Tenório and D.C.R.J.B.J.o.C.E. Espinosa, 32 (2015) 831.
[107] C.J.A.J. Bennett, 12 (1966) 204.
[108] R. Huggins, Advanced batteries: materials science aspects, Springer Science & Business Media, 2008.
[109] A.J. Bard, L.R. Faulkner, J. Leddy and C.G. Zoski, Electrochemical methods: fundamentals and applications, wiley New York, 1980.
[110] A.J. Bard and L.R.J.E.M. Faulkner, 2 (2001) 482.
[111] D. Pletcher, A first course in electrode processes, Royal Society of Chemistry, 2009.
[112] J. Newman and K.E. Thomas-Alyea, Electrochemical systems, John Wiley & Sons, 2012.
[113] D. Reddy, J.C. Bolivar, K.J.P.P.o.S.D. Sobhan and Construction, 18 (2012) 225.
[114] S. Xu, Y. Kim, D. Higgins, M. Yusuf, T.F. Jaramillo and F.B.J.E.A. Prinz, 255 (2017) 99.
[115] J.H. Shim, J.E. Kim, Y.-B. Cho, C. Lee and Y.J.P.C.C.P. Lee, 15 (2013) 15365.
[116] M.A. O'Keefe, L.F.J.M. Allard and Microanalysis, 10 (2004) 1002.
[117] J. Zhang, PEM fuel cell electrocatalysts and catalyst layers: fundamentals and applications, Springer Science & Business Media, 2008.

[118] P. Rieger and P.-H.J.á.S.á. Electrochemistry, 343.
[119] C.-L. Sun, H.-H. Lee, J.-M. Yang, C.-C.J.B. Wu and Bioelectronics, 26 (2011) 3450.
[120] S.T. Nguyen, D.S.L. Tan, J.-M. Lee, S.H. Chan, J.Y. Wang and X.J.i.j.o.h.e. Wang, 36 (2011) 9645.
[121] S. Çete, A. Yaşar, F.J.A.c. Arslan, blood substitutes, and biotechnology, 34 (2006) 367.
[122] T. Jarvi, S. Sriramulu, E.J.C. Stuve, S.A. Physicochemical and E. Aspects, 134 (1998) 145.
[123] N. Matei, S. Birghila, V. Popescu, S. Dobrinas, A. Soceanu, C. Oprea and V. Magearu, Rom. J. Phys, 53 (2008) 343.
[124] L. Yan, A. Brouzgou, Y. Meng, M. Xiao, P. Tsiakaras and S.J.A.C.B.E. Song, 150 (2014) 268.
[125] J. Huang, Y. Liu, H. Hou, T.J.B. You and Bioelectronics, 24 (2008) 632.
[126] F. Tzorbatzoglou, A. Brouzgou and P.J.A.C.B.E. Tsiakaras, 174 (2015) 203.
[127] A. Brouzgou, L. Yan, S. Song and P.J.A.C.B.E. Tsiakaras, 147 (2014) 481.